> <

*

Statistical comparison of ocean wave directional spectra derived from SWIM/CFOSAT satellite observations and from buoy observations

Ying Xu, Danièle Hauser, Jianqiang Liu, Jianyang Si, Chen Yan, Shufen Chen, Junmin Meng, Chenqing Fan, Meijie Liu, Ping Chen

***Abstract*—The comparison and verification of ocean wave spectrum by remote sensing and by in-situ measurements at the spectral level is quite rare, because the use of the traditional comparison method lead to very limited spatio-temporal matching pairs. In this paper, a new comparison method is proposed. With this method, under different sea conditions (wind wave mainly/swell mainly) and sea surface conditions (wind speed smaller than 20m/s, significant wave height from 1m to 7m), mean directional wave height spectra from SWIM (Surface Waves Investigation and Monitoring) are compared at the spectral level to the buoy counterparts, in different classes of sea-state. This includes the comparison of the omni-directional wave height spectrum and the directional function at the peak wave number. The comparison results show that under medium and high sea conditions, wave directional spectra provided by the SWIM beams at 8 ° and 10 ° incidence have a high consistency with those from buoy data. Under low sea conditions, the measurement bias of SWIM wave directional spectra mainly comes from three phenomena which are, by order of importance, an abnormal lifting of spectral energy caused by non- wave components at low wave numbers (parasitic peak), from the non-linear surfboard effect in the radar imaging mechanism and from a slight underestimation of speckle noise spectral density.**

***Index Terms*—spaceborne radar, scatterometer, omni-directional wave height spectra, directional function, directional spread**

I. Introduction

The measurement of ocean wave directional spectrum is important for marine meteorology, navigation, offshore and coastal activities, as well as to validate the wave models, to promote the analysis of wave physics and air-sea interaction processes. SAR (Synthetic Aperture Radar) can provide wave spectra over the ocean, but with frequent smearing and distortion effects, in particular for waves shorter than about 200m when they propagate close to the along-track directions. This is due to the non-linear imaging mechanism associated with to the velocity bunching effect [1][2]. The wave scatterometer [3] is a RAR (Real Aperture Radar) system with a near-nadir scanning beam geometry, specially designed to measure the spectral properties of surface ocean waves. Compared with SAR, wave scatterometer observations are not affected by the velocity bunching effect and thus much less limited in the detection of wind waves. The wave scatterometer SWIM (Surface Waves Investigation and Monitoring) carried by CFOSAT (China France Oceanography Satellite) is the first space borne wave scatterometer, with which the world-wide directional spectra of ocean waves are produced systematically since end of April 2019. As SWIM is a recent concept for space missions, a careful assessment of its performances and limits is required.

Since the first SWIM data set was delivered, several studies have been carried out to assess the wave spectra products. In particular, [4], and [5] present the performance of wave parameters, such as the significant wave height (SWH), peak wavelength, dominant wave direction, angular spread of the dominant waves, calculated from the SWIM wave spectra and compared to independent data sets. In these studies, the main source of reference was wave parameters from numerical wave models, even if buoy data were marginally used in [5]. [6] conducted a comparison study between significant wave height from SWIM off-nadir wave spectrum and those from SWIM nadir beam, from buoy data and from Jason-3 altimeter data. Because the number of matching pairs between SWIM and buoy data is small, so the indicators of the significant wave height comparison of SWIM off-nadir beam and buoy data, such as deviation and mean square deviation are worse than

The CFOSAT data are provided by courtesy of the China National Space Administration (CNSA) and Centre National D'Etudes Spatiales (CNES).This work was supported in part by the National Natural Science Foundation of China under Grant 42176184, Grant 41976168, Grant 41976173, in part by the Shandong joint fund of National Natural Science Foundation of China under grant U2006207, in part by the Shandong Provincial Natural Science Foundation, China, ZR2019MD016 and GASI Project under contract No. GASI-01-DLYG-WIND01, and the Dragon-5 Cooperation Project ID. 59310 . (Corresponding author: Ping Chen, e-mail: chenping@hust.edu.cn)

Ying Xu and Jianqiang Liu are with National Satellite Ocean Application Service, Beijing 10081, China.

Danièle Hauser is with LATMOS, Université Paris-Saclay, UVSQ, CNRS, Sorbonne Université, Guyancourt, France.

Jianyang Si, Chen Yan, Shufen Chen and Ping Chen are with School of Electronic Information and Communications, Huazhong University of Science and Technology, Wuhan, China.

Ying Xu and Jianqiang Liu are with Key Laboratory of Space Ocean Remote Sensing and Application, Ministry of Natural Resources, Beijing 100081, China.

Ying Xu is with Southern Marine Science and Engineering Guangdong Laboratory, Guangzhou 511458, China.

Junmin Meng and Chenqing Fan are with First Institute of Oceanography, Ministry of Natural Resources of China, Qingdao, China.

Meijie Liu is with College of Physics, Qingdao University, Qingdao, China.

those for the comparison of SWIM off-nadir beam and SWIM nadir beam, or Jason-3 altimeter data.

The main conclusion of these studies is that SWIM observations from beam 10° give the best results, while the beam 6° gives the less satisfactory results. This was explained by the fact that the beam 10° has the smallest contribution of speckle noise contribution (largest number of averaged echoes). However, when no normalization is applied in the conversion of the signal modulation spectra to wave slope spectra (Modulation Transfer Function called MTF-1), SWH is overestimated at wave heights smaller than 2 to 3m and underestimated at larger wave heights. This shortcoming, was partially attributed to the presence of a parasitic peak at low wave number, to remaining uncertainties in the noise correction and to the MTF estimation [4]. This motivated the use of an alternative MTF which consisted in normalizing the directional spectra so that the corresponding SWH (estimated from the integrated energy over wave number and directions) corresponds to the SWH measured from the nadir beam (as provided classically by altimeter mission observations). According to these previous studies, the direction of the waves and the dominant wavelengths are generally well retrieved except in some of the conditions where waves propagate in the along-track sector. According to [4], the rms differences for the dominant direction and wavelength with respect to the reference (MFWAM wave model) were found of the order of 16° to 27° and 23m to 45 m, respectively, depending of the method of analysis. More recently, [7], find from a combined analysis of wave partitions from SWIM and buoys that the rms difference in the spectral peaks between both sources of information are of 0.9 s for the peak period and 20° for the direction. However, [8] in a study limited to the South China Sea find important biases on the peak wavelength from SWIM compared to buoy measurements in low sea state conditions.

In order to better characterize the conditions where the SWIM observations are consistent with buoy observations and what explains the differences when these exist, we have developed a new method to compare the SWIM wave spectral properties with those provided by buoy measurements. The originality of our method is that instead of carrying out comparisons from a SWIM/buoy spatio-temporal matching data set, we choose here a method based on mean spectra estimated for different classes of sea-state conditions, i.e., different classes of wind sea and swell conditions. The interest of this approach is to overcome the difficulty to gather a large statistics of time-space matching pairs. Furthermore, it is useful to analyze the optimal conditions where we can be confident in the SWIM data. The other originality of our study is to compare not only the main parameters of the wave spectrum (such as significant wave height, peak wavelength and peak direction), but also the details of the spectral information, based on the analysis of the omni-directional spectra, on the wave spectra in the dominant wave propagation direction and on the angular distribution of wave energy at the spectral peak.

In section II, we present a method developed to compare wave height spectrum obtained from SWIM and from the buoys, the data sets used in our study, the sea state classification and the pre-processing methods developed for the comparisons. In sections III and IV, we present the comparisons between SWIM and buoy data for respectively, the wave height omni-directional spectra and the directional function at the peak wave number. The conclusions are drawn in section V.

II. Data and method

In the following, firstly we propose a method to compare SWIM data with buoy data (section II-A). This method does not need a direct spatio-temporal matching between buoy and SWIM data sets. Then we describe three data sets used in the comparison method, the buoy data set used as reference (section II-B), the SWIM data set (section II-C), and the wave model data MF_WAM used to build the different classes of sea-state conditions (section II-D). In section II-E we present the different classes of sea-surface conditions retained in our analysis. In sections II-F to II-H we describe how we estimate and compare between SWIM and buoy the two quantities considered in the comparisons (omni-directional and directional function).

A. Comparison method

In order to make comparisons from satellite and in situ data correspond to the same sea surface conditions, people generally adopt the method of space-time matching, that is, set a certain time and space window, assume that the sea surface conditions remain unchanged in this space-time window, and then collect the measured data and reference data in this space-time window for comparison. However, this spatio-temporal matching method is not well adapted for the comparison of SWIM and buoy wave spectrum data, because SWIM has only been in orbit for three years, the number of samples successfully matched in spatio-temporal with buoy measurements is small, and these samples also correspond to different sea surface conditions. In other words, corresponding to a specific sea surface condition, the sample size satisfying spatio-temporal matching is rather small. Then such a statistical comparison will suffer from a large statistical uncertainty due to the sample size of both SWIM and reference data. In order to solve this problem, we considered an alternative method, which ensures that the measured and reference data involved in the comparison correspond to the same sea surface conditions.

Firstly, we assume that for a given sea state condition (dominated by either wind sea or swell) and surface condition parameters (wind speed, wave age, significant wave height and peak wavelength), the wave directional spectrum is independent of time and location. If this assumption is valid, then under the same sea state and sea surface parameters, we can collect large number of the wave spectrum measurement samples obtained at different times and places, and for buoy and SWIM separately. Therefore, we can break the limitation of space-time matching mentioned above, and gather a large number of spectrum samples for the validation.

Here we consider under what conditions the above assumption may not be true. We know that in addition to the above sea surface parameters, water depth and strong current

will also affect the wave spectrum. Therefore, in the following analysis, we exclude the strong current areas and select the deep-water areas.

Secondly, for a same couple of Hs and peak wavelength λ_p (or peak wavenumber k_p), the wave spectra may still correspond to different wave components (wind sea, swell conditions). In order to ensure that buoy data and SWIM data are compared under exactly the same sea surface conditions, only the conditions with a single wave component are further selected. Therefore, only the samples with the main wave component energy accounting for more than 90% of the total energy are selected. The method to separate data in either wind sea or swell categories is described in section II-E.

When collecting buoy data that meet the requirements, in addition to the above sea surface conditions provided by the buoy data parameter, we also use the information on different wave partitions to select those samples with relatively single wave component. Here, we analyze the MFWAM wave parameters of the different wave partitions and select conditions corresponding to a single wave component. Then, through a spatio-temporal matching of MFWAM and buoy data, we associate this single wave component condition to the buoy data (see also section II-E). Similarly, by matching MFWAM and SWIM data, we apply the same method to select SWIM samples having only one wave component. It is noted that as the wind vectors are not provided in the MFWAM products, we take the wind vectors corresponding to each SWIM measurement from the "SWIM AUX" data products, which contain the ECWMF 6-hour forecast winds [9]. Using these wave parameters and wind vectors, we obtain a set of SWIM directional spectra corresponding to a single wave component, for each sea state and surface condition (wind speed, significant wave height and peak wavelength).

Thirdly, in order to reduce the influence of the statistical fluctuation on the validation, all samples of buoy (or SWIM) with the same sea surface condition are averaged. Finally, the average wave spectra obtained from SWIM are directly compared with those obtained from the buoys under different sea state conditions. Both buoy and SWIM provide directional spectra (2D spectra), however, direct comparison of 2D spectrum is not trivial. So, we made the comparison on the omni-directional wave height spectrum and the directional function at the peak wave number in azimuth.

Instead of direct spatio-temporal matching between buoy and SWIM data sets, the presented method takes the same sea state and sea surface parameters as classification conditions for buoy and SWIM measurement. Because a single buoy measurement sample always contains a certain error, we set the parameter variation range of a given sea surface parameter within the buoy measurement error. For example, we set the significant wave height H_s bins as $(H_{s0} \pm 0.1H_{s0}\ \ H_{s0} - 0.1H_{s0}, H_{s0} + 0.1H_{s0})$, where H_{s0} is the central value of H_s for that sea condition. The ratio of 0.1 is from measurement error for buoy 10%. By this setting, the presented method can almost achieve the same verification reliability as traditional space-time matching method.

B. NDBC buoy data

The buoy data used in this study come from NDBC buoy data sets provided by the National Oceanic and Atmosphere Administration (NOAA). The buoy parameters used here are wind speed, significant wave height, peak period, dominant wave direction, energy density spectrum $C_{11}(f)$ at 47 wave frequencies f from 0.04 Hz up to 0.4850 Hz [10], the ratio of the normalized Fourier coefficients $R_1(f)$, $R_2(f)$, mean wave direction $\phi_1(f)$, and dominant wave direction $\phi_2(f)$.

From the spectral data product a two-dimensional wave height spectrum $F_{buoy}(f,\phi)$, can be reconstructed as the product of the energy density spectrum $C_{11}(f)$ and the directional function $D(f,\phi)$:

$$F_{buoy}(f,\phi) = C_{11}(f) * D(f,\phi) \quad (1)$$

We employed the Maximum Entropy Method (MEM) proposed in [11] to reconstruct the two-dimensional wave spectra from estimates of the Fourier coefficients. A sampling interval of 15° was chosen to be compatible with the SWIM data (see below).

The directional spread in the energy containing part is an important feature of the wave spectra. The directional spread ($\Delta\phi$) can be calculated by $D(f,\phi)$ [24]

$$\Delta\phi(f) = \sqrt{\int_0^{2\pi}(\phi - \phi_0)^2 \cdot D(f,\phi)d\phi} \quad (2)$$

Where ϕ_0 is the mean wave direction. $\Delta\phi(f)$ can be approximated using the coefficients of Fourier series a_1 and b_1, provided by buoy [24, 25]

$$\Delta\phi(f) = \sqrt{2(1 - (a_1^2 + b_1^2)^{\frac{1}{2}})} \quad (3)$$

It is important to note for the discussion that will come in Section IV that we have checked that $\Delta\phi(f)$ estimated from (3) with the Fourier coefficients a1 and b1 taken from the NDBC files or estimated from (2) after we have estimated $D(f,\phi)$ with the MEM method are exactly the same.

Considering the influence of sea depth on wave spectrum, 44 NDBC buoy sites in deep water (water depth >200 m, distance from coastline > 50km) were selected in this paper, and the time coverage was from January 2019 to December 2020.

In order to compare spectral data between NDBC and SWIM observations, it is necessary to transform the wave spectra from the buoy expressed as a function of frequency into wave height spectra expressed as a function of wave number. This is done by applying the dispersion relationship in deep water, considering that the 44 NDBC buoy sites are in deep water (water depth >200 m)

$$F(k) = C_{11}(f)/\left(\frac{8\pi^2 f}{g}\right) \quad (4)$$

In addition to converting the buoy spectrum into a wave number spectrum, a resampling is also applied in order to get the same sampling in wavenumber for both SWIM and buoy data for the calculation of correlation coefficient (see II-H): the buoy wave height density is linearly interpolated on a wavenumber grid k_i with a wavenumber interval of Δk over the wavenumber range (k_{min}, k_{max}). Here k_{min}, k_{max} is set as the common measurement range of wave numbers by SWIM and buoy, i.e., k_{min}=0.0126 and k_{max}=0.28 rad/m, and Δk is set as 0.0002.

Note that the dominant wave number from the buoy data is not recalculated after these conversions, but taken from the peak period provided in the buoy files and then converted into dominant wavenumber using the dispersion relation in deep water (water depth >200 m).

C. SWIM Data Set

CFOSAT SWIM is a Ku-Band radar with a multi-incidence and scanning azimuthal geometry [4]. It illuminates the surface sequentially with 6 incidence angles: 0°, 2°, 4°, 6°, 8° and 10°, each beam with a beam aperture in elevation and in azimuth of 1.5° to 1.8°. Given the orbit height, the footprint dimension of each beam is about 18 km×18 km, and the full swath for the outer beam (10°) is about 90 km in radius. In order to acquire data in all azimuth directions, the antenna beam is rotated at a speed rate of 5.6 rpm, which generates, when combined with the satellite advection, some overlap in the sampling of successive rotations. Off-nadir beams at 6°, 8°, 10° are called the "spectral beams", as observations from these beams are used for estimating the 2D wave spectra and wave spectra parameters. Each 2D spectrum is constructed from observations of successive overlapping antenna scans over 180° (on each side of the track), and representative of wave cells (boxes) of about 70×90 km.

The data products used in this paper are L1b and L2 SWIM products (version-5.1.2) from 1st Jan., 2021to 28th Feb., 2021 provided by the China National Space Administration (CNSA). Using the rainfall information provided by GPM_3IMERGHH data product [12] and the sea land signs and sea ice coverage information provided by SWIM AUX data products, the rain free marine scene data are screened out from the SWIM data products. For the reasons described in section II-A, the data of strong current areas (speed>1 m/s) is removed with daily surface currents provided by CMEMS (Copernicus Marine Service),
GLOBAL_ANALYSISFORECAST_PHY_CPL_001_015.

As intermediate products for the generation of wave spectra, L1b product provides radar cross section modulations, and modulation spectral density, impulse response function and speckle density spectrum, for each SWIM look direction and for the 6°, 8°, 10° beams [4], [13]. In this work, time and location from each macro-cycle in L1B products (i.e., from each sample in azimuth) are used for matching SWIM and MFWAM data.

The L2 products provided with version-5.1.2 are wave slope spectra estimated using a Modulation Transfer Function (MTF) which forces the significant wave height H_s to be equal to the significant wave height provided by the nadir beam (this latter is estimated from the nadir waveform similarly to altimeter missions, see [14]. This choice was done after Hauser et al, 2021, showed that the initial MTF (called MTF1) based on the use of the normalized radar cross-section measured by SWIM, induced biases on H_s. However here, we go back to this initial version of the MTF because we are interested in assessing the SWIM spectra in the version when their energy is not constrained by an additional information.

So the wave slope spectra $S(k,\phi)$ have been re-estimated from the L2 modulation spectra $P(k,\phi)$ using (see [13], [4]):

$$S(k,\phi) = P(k,\phi)/\,MTF(\theta,\phi) \tag{5}$$

L2 modulation spectra $P(k,\phi)$ for 6°, 8°, 10° incidence provided by L2 data is over 12 bins of azimuth angle ϕ from 0° to 180° (with an ambiguity of 180°), and over 32 wave number k bins unequally spaced from k_{min}=0.0126 to k_{max}=0.28 rad/m (with width *dk* of each wavenumber bins following *dk/k*=10%).

With

$$MTF(\theta,\phi) = \frac{\sqrt{2\pi}}{L_y}\left(ctg\theta - \frac{1}{\sigma^0}\frac{\partial\sigma^0}{\partial\theta}\right)^2 \tag{6}$$

Where σ^0 is the normalized radar cross-section changing with the incidence angle and azimuth angle, σ^0 is taken here from the variable named "sigma0_mini_profile"in L2 data, θ the incidence angle (6°, 8°, 10°) and L_y a geometric factor related to the width of the footprint in azimuth (see [13]).

Then the wave height spectrum $F(k,\phi)$ is calculated according to its definition by:

$$F(k,\phi) = \frac{S(k,\phi)}{k^2} \tag{7}$$

The omni-directional wave height spectrum, $F(k)$ is then calculated as the polar integral over $kd\phi$ of the 2D spectrum $F(k,\phi)$:

$$F(k) = \int_0^{2\pi} F(k,\phi)kd\phi \tag{8}$$

With our conventions, the directional function $D(k,\phi)$ is related to the directional spectrum by:

$$F(k,\phi) = \frac{1}{k}F(k)D(k,\phi) \tag{9}$$

With

$$\int_0^{2\pi} D(k,\phi)d\phi = 1 \tag{10}$$

In this work, besides 2D modulation spectrum of spectrum beams, dominant direction ϕ_p and dominant wavelength λ_p of the total wave spectra provided in wave boxes are used to generate, for the comparison of the directional function at the peak wave number k_p. It is noted that in these products, the dominant wavelength and dominant directions are estimated from the peak energy of the wave slope spectrum expressed as a function of wavenumber and azimuth angle.

D. MFWAM Data Set

The MFWAM is the French version of the third generation wave model WAM model. It is based on the ECMWF version (referred as ECW AMIFS-38R2) with a parameterization taken from the ST4 version of the WW3 model [15]. The MFWAM wave model takes into account the interaction between waves and ocean currents. The MFWAM wave model assimilates the significant wave heights of spaceborne altimeters (e.g., Jason 2, Jason 3, Saral, Cryosat-2) and the spectral information from the spaceborne synthetic aperture radar (Sentinal-1a, Sentinal-1B) and the spectral information from SWIM since February 2nd, 2021. The MFWAM wave model is driven by the wind field of the IFS-ECMWF atmospheric system (with a time resolution of 3h) and its wave product has a grid size of 10km. The MFWAM reanalysis data product has a time resolution of 3h and a spatial resolution of 0.0833°×0.0833° (latitude and longitude).

The MFWAM data used in this paper are wave parameters of the total sea and of different wave components, namely, the most energetic swell (called 1st swell), the second energetic

swell (called 2nd swell) and the wind waves. Three wave parameters of the total sea are used: significant wave height, peak wave period and dominant wave direction. The wave parameters of the wave components include the significant wave height, mean wave period and mean wave direction. Here, both dominant direction of the total sea and mean directions of the partitions are relative to the geographic North.

E. Sea state classification

The sea state classification adopted here is based on several criteria. First wind sea and swell are considered as two main categories (see below for the details). We avoid mixed sea conditions by retaining samples for which one of the conditions largely dominates (i.e., represents at least 90% of the total wave energy). Then different subcategories are defined. For wind sea, we separate young wind sea, developed wind sea and mature wind sea as is explained further down. Then, within each of these subcategories, the data are analyzed within different classes of wind speed. As for the swell category, 3 different subcategories are defined according to the peak wavenumber of the spectra, and in each of these subcategories, the data are classified according to their significant wave height. The list of classes is presented in Table 1, whereas details about the method used to construct these classes are explained here below.

For SWIM data, the separation of wind sea and swell needs external data, in particular information on wind. We choose here to use ancillary data provided by the MFWAM model (see section II-D).

Firstly, SWIM sample of the L1B product (each macro cycle contained a wave box) is spatiotemporal matched with MFWAM to obtain the MFWAM wave parameters corresponding to each macro cycle. Considering the 3h time resolution of MFWAM data, and the spatial resolution of 0.0833°×0.0833° (i.e. , About 9km at the equator), we choose a time window of ±1.5h for matching SWIM and MFWAM data. Within this time window, the location points of MFWAM closest in longitude and latitude to each macro-cycle measurement provided by the SWIM L1B products are matched (equivalent spatial window $4.5\sqrt{2}$ km). Then all the MFWAM parameters of grid points matched within a box of SWIM L2 product are averaged to obtain the collocated MFWAM data for this box. This matched data set covers the period from 1st Jan., 2021to 28th Feb., 2021 and covers the global scale.

In order to separate wind sea from swell, have used the following criterion, based on two parameters, a dimensionless height variance η^* and the inverse wave age Ω as proposed by [16] and also used by [17]:

$$\eta^* = \eta^2 g^2 / U_{10}^4 \quad (11)$$

$$\Omega = \omega_p U_{10} \cos\theta' / g \quad (12)$$

here η is the sea surface standard deviation ($\eta = H_s/4$) ω_p is the peak angular frequency ($\omega_p = \sqrt{g k_p}$) , θ' is the angle between the wind and the dominant wave direction, g the gravitational acceleration. Note that the inverse wave age Ω accounts for the cases when dominant waves are not aligned with the wind direction. Here, H_s and k_p are respectively the total significant wave height and peak wave number provided by MFWAM in the above matching data set. U_{10} is the ECMWF IFS wind speed at a height of 10m above the sea surface, which is provided by the ancillary meteorological SWIM products. The same ECMWF IFS winds were used in the MFWAM model runs.

Following the criteria used by [16] and [17], we define several types of situations

1.Situations dominated by swell (pure swell or dominant swell):

$$\eta^* > 3.64 * 10^{-3}, \text{ and } \Omega < 0.84 \quad (13)$$

2.Pure wind waves:

$$\eta^* \leq 3.64 * 10^{-3}, \text{ and } \Omega > 0.84 \quad (14)$$

After sea state classification of the matched SWIM/MFWAM data set according to the above classification conditions, to avoid conditions of mixed seas for which the intercomparison results may be more difficult to interpret, the SWIM data with the main wave component energy accounting for more than 90% of the total energy are selected according to the partition parameters provided by MFWAM data.

To build the different classes from the NDBC data set, we first match in time and space the MFWAM and buoy data (from January 2019 to December 2020) and then gather the buoy samples for each category relative to the different conditions according to buoy data, and finally we select those samples with the main wave component energy accounting for more than 90% of the total energy according to MFWAM partition data.

In the following, the comparisons are presented for the swell and wind sea conditions, in different subclasses as summarized in Table 1 where k_p is selected to correspond to the peak wavenumber of the buoy measurements, λ_p the corresponding wavelength, H_s the significant wave height, δ the significant slope $\delta = H_s/\lambda_p$. The number of the colocation pairs for buoy/MFWAM and SWIM/MFWAM, N_{Buoy} and N_{Swim}, respectively, are also list in Table 1.

TABLE I
Sea Surface Conditions In Verification

Wind wave	Developing $\Omega = 1.3$	U_{10} (m/s)		12	14	16	18	20
		$H_s(m)$		1.77	2.51	3.19	4.59	5.54
		δ		0.0326	0.0316	0.0347	0.0354	0.0354
		N_{Buoy}		179	388	250	242	141
		N_{Swim}		67	213	131	242	96
	Mature $\Omega = 1$	U_{10} (m/s)	10	12	14	16	18	20
		$H_s(m)$	1.79	2.56	3.58	4.59	6.12	7.61

> <

		δ	0.0295	0.0277	0.0277	0.0294	0.0300	0.0293
		N_{Buoy}	280	785	752	385	176	54
		N_{Swim}	81	371	858	810	623	339
	Fully developed $\Omega = 0.84$	U_{10} (m/s)	10	12	14	16	18	
		$H_s(m)$	2.35	3.39	4.62	5.68	7.86	
		δ	0.0254	0.0263	0.0253	0.0248	0.0265	
		N_{Buoy}	359	509	180	121	61	
		N_{Swim}	106	410	308	327	150	
swell	$k_p = 0.0133$ m^{-1}, $\lambda_p = 472$ m	$H_s(m)$	2.5	3,5	4.5			
		δ	0.0053	0.0074	0.0095			
		N_{Buoy}	102	128	145			
		N_{Swim}	201	352	366			
	$k_p = 0.0157$ m^{-1}, $\lambda_p = 400$ m	$H_s(m)$	2	3	4	5	6	7
		δ	0.005	0.0075	0.0100	0.0125	0.0150	0.0175
		N_{Buoy}	162	209	243	169	129	61
		N_{Swim}	218	527	815	741	474	222
	$k_p = 0.0211$ m^{-1}, $\lambda_p = 298$ m	$H_s(m)$	2	3	4	5	6	7
		δ	0.0067	0.0101	0.0134	0.0168	0.0201	0.0235
		N_{Buoy}	499	792	587	341	178	50
		N_{Swim}	810	2026	2107	1243	377	70
	$k_p = 0.0308$ m^{-1}, $\lambda_p = 204$ m	$H_s(m)$	2	3	4	5		
		δ	0.0098	0.0147	0.0196	0.0245		
		N_{Buoy}	807	699	310	60		
		N_{Swim}	1131	2491	1281	157		
	$k_p = 0.0580$ m^{-1}, $\lambda_p = 108$ m	$H_s(m)$	1	2	2.5			
		δ	0.0092	0.0185	0.0231			
		N_{Buoy}	1156	890	220			
		N_{Swim}	53	300	90			

For each specified sea surface condition with parameter U_{10}, k_p and H_s, the variation range considered for these sea surface parameters are set as ± 2m/s for U_{10} , $\pm 0.1 k_p \; for \; k_p$, $\pm 0.1 H_s \; for \; H_s$, these last two intervals being of the order of buoy measurement error.

F. Omni-directional wave height spectra

An example of a mean omni-directional wave height spectrum from SWIM and from the NDBC buoys is shown in Fig. 1(a) and 1(b) respectively, for the swell case with significant wave height 3m, peak wavenumber 0.0308rad/m. For each wavenumber, the box plots in these figures show the distribution of spectral values and the mean values (see the legend of Fig.1). Fig.1(c) and 1(e) show the mean and Inter Quartile Range (IQR) of spectral values for SWIM and buoy data, respectively. In these plots, the spectra are kept with their original sampling in wavenumber.

The number of samples gathered in these examples is 699 for buoy and 2476, 2485 and 2491 SWIM beam 6°, 8° and 10°, respectively.

Fig. 1(a) shows that for both buoy and SWIM measurements, the mean value for wavenumbers less than 0.0253 rad/m is slightly larger than the median value, while the mean value for wavenumbers larger than 0.0253 rad/m is almost equal to the median value. It indicates that spectral values for both buoy and SWIM are close to normal distribution except just a little skewed to the right for wavenumbers less than <0.0253 rad/m. From Fig. 1(a) it can be seen that in the small wavenumber range, both the mean and the IQR corresponding to the 6° beam spectrum is larger than those corresponding to the 8°, and 10° beam spectra, while at wavenumbers larger than the peak wavenumber, the mean spectrum values from the 6° beam are smaller than those from the 8° and 10° beams. However, the wavenumber corresponding to the energy peak is consistent between the three SWIM beams. By comparing Fig. 1(a) to Fig. 1(b), we can also conclude that the spectral level at small wavenumbers (<0.0187) can be considered as a non-wave contribution and that the 6° beam is more sensitive to this artefact than the 8°, 10° beams.

As shown in Fig. 1(a), the range of energy density variation observed from the SWIM data is quite large. In order to filter out abnormal spectrum samples, in the analysis discussed in sections III to V, a Tukey's test on the integral value of each spectrum sample is applied: a spectrum sample is removed if its integral value integrated over the wavenumber range [0.0126 rad/m, 0.28 rad/m] is outside 1.5 × IQR from the lower and upper quartile.

Note that the number of SWIM samples in Fig. 1(a) is quite different from that of buoy samples in Fig. 1(b), because they come from different data sets. In order to investigate the impact of different sample size on the comparison results, we randomly selected 699 samples from the 2476, 2485 and 2491 SWIM

samples for the three beams respectively to compare results with same sample size for SWIM and buoy. Fig.1 (d) and Fig.1 (f) show the comparison between SWIM and buoy data for the spectral mean and spectral IQR, respectively when the sample size is the same. From Fig.1 (c) and Fig.1 (d), it can be concluded that the size of SWIM samples barely influences the averaged spectrum: the wavenumber corresponding to the maximum spectral value is exactly the same, and the change of this maximum value with different sizes of the SWIM data sets is 0.7%, 0.8% and 0.5% for beams 6°, 8°,10°, respectively. Therefore, the comparison method based on averaged spectrum estimated on a different number of samples is reliable and well adapted to the different nature of the two sample sets. As for Fig.1 (e) and Fig.1 (f), it is interesting to note that the curves of IQR follow those of the mean wave height spectra, indicating that the statistical uncertainty is related to the spectral level. IQR of all the three SWIM beams for SWIM sample sizes of 2476, 2485 and 2491 is similar to that for the sample size of 699 with the relative difference of IQR peak of 3.0%, 6.6%, 1.7% for beams 6°, 8°, 10°. It means that the sample size only slightly impacts the variation range of the spectral random variable.

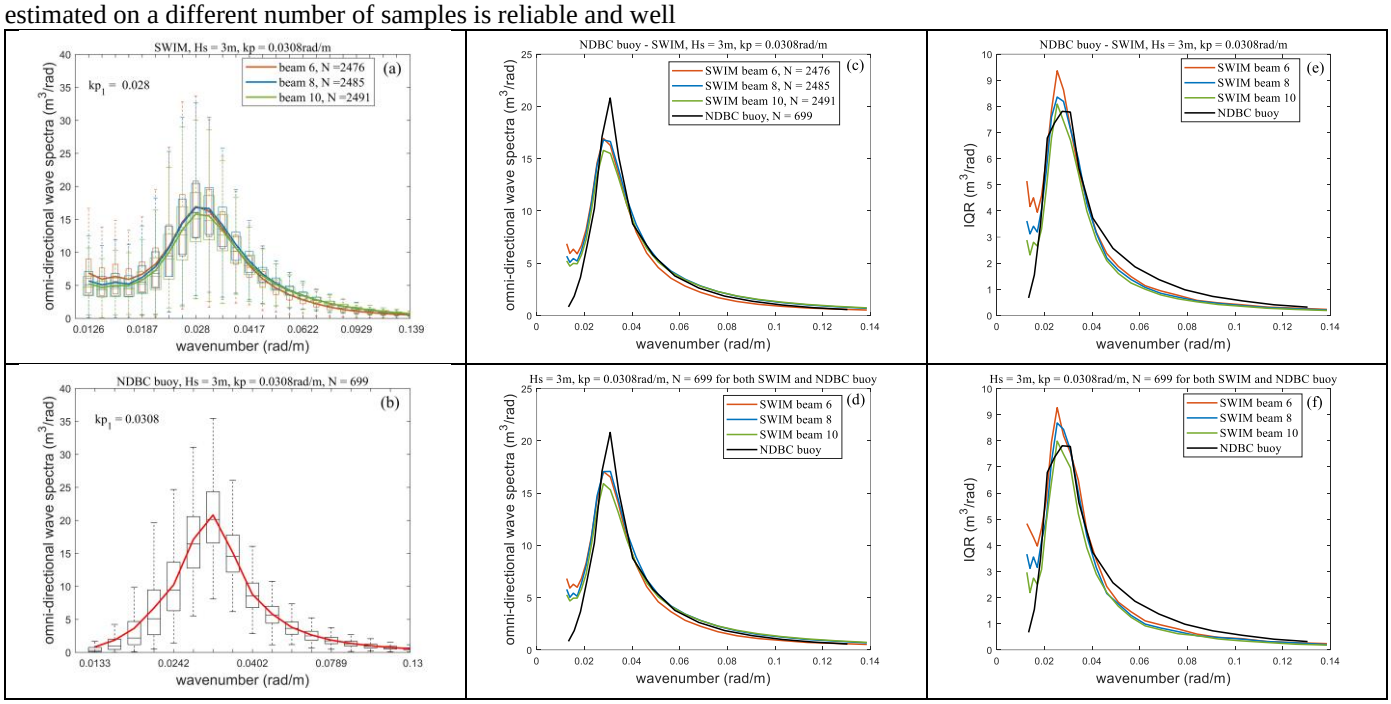


Fig. 1. Distribution of the omni-directional spectral density as a function of wavenumber for SWIM (Fig.1(a)) and for buoy (Fig.1(b)), averaged density spectra for SWIM beams and for buoy (Fig.1(c)) averaged density spectra of random 699 samples for all SWIM beams (Fig.1(d)), and Inter Quartile Range (IQR) (Fig.1(e) and Fig.1(f)). This illustration is given for the category of swell with H_s 3m, peak wavenumber 0.0308 rad/m. The central boxes in Fig.1(a) and (b) also represent IQR and the whisker extends to the largest and smallest data value within 1.5 × IQR from the lower and upper quartile, respectively. In Fig.1 (a), the box plots (thin lines) and the mean spectrum values (thick curves) of 6°, 8°, 10° are shown in red, blue and green, respectively. The same color code is adopted for SWIM values in Fig.1(c) and (d) and black curves are for buoy values, in Fig. 1(e) and (f). In Fig.1 (b) the box plots and the mean spectrum values are in black and red.

In the following we analyze average spectra in the different classes of sea state as defined in Table 1. A direct averaging of the spectral energy density may induce a reduction and/or broadening of the peak energy because the peak wave number may vary from one sample to another one. Therefore, we carried out the spectrum average by first normalizing the wave number for both buoy and SWIM measurements as explained below. It is assumed that the independent spectra from SWIM or buoy are given for each element of the wavenumber vector k_{spec}, defined over N_k elements. And two variables dk_{spec} and $k_{bin}(i)$ are defined.

$$dk_{spec}(i) = k_{spec}(i+1) - k_{spec}(i), i = 1,2, \ldots, N_k - 1, dk_{spec}(N_k) = dk_{spec}(N_k - 1) \quad (15)$$

$$k_{bin}(j) = \left[k_{spec}(j) - \frac{dk_{spec}(j)}{2}, k_{spec}(j) + \frac{dk_{spec}(j)}{2}\right], j = 1,2, \ldots, N_k. \quad (16)$$

For a spectrum n of a given class of N samples, we assume its wavenumber at the maximum value to be $k_{p1}(n)$, and we can calculate the normalized wavenumber vector, and the averaged peak wavenumber of a certain sea-state class by:

$$k_{norm}(i,n) = \frac{k_{spec}(i)}{k_{p1}(n)} \quad (17)$$

$$k_{pmean} = \frac{\sum_{n=1}^{N} k_{p1}(n)}{N} \quad (18)$$

Then the normalized wavenumber bin of a certain sea state is defined by:

$$k_{bin-norm}(i) = \frac{k_{bin}(i)}{k_{pmean}} \quad (19)$$

The next thing to do is to find the normalized wavenumber interval $k_{bin-norm}(i)$ where each normalized wavenumber of

the sample $k_{norm}(j,n)$ is located, accumulate its spectral value $spec(j,n)$ in this interval and count. Therefore, the spectrum as a function of the normalized wavenumber is expressed as:

$$spec_{mean}(i) = \frac{\sum_{j=1}^{j=N_k}\sum_{n=1}^{n=N} spec(j,n), k_{norm}(j,n)\in k_{bin-norm}(i)}{Number\ of\ k_{norm}(j,n)\in k_{bin-norm}(i)} \quad (20)$$

Finally, we need to convert the independent variable from normalized wavenumber k_{norm} back to wavenumber k. We find the wavenumber bin in which k_{pmean} lies and name it $k_{bin}(p)$, i.e., $k_{pmean} \in k_{bin}(p)$, then k is determined by:

$$k = \frac{k_{spec}}{k_{spec}(p)} * k_{pmean} \quad (21)$$

The main difficulty of the method presented above is the determination of the maximum value for each sample. In particular for low sea state classes, there are important fluctuations in the spectral density so that an accurate maximum value may be hardly found. Besides, the parasitic peak also influences the determination of the peak. Therefore, we constrained the range of wavenumber to find the peak within a range which varies with sea state. For example, when the peak of signal containing part is a little smaller than the parasitic peak, we search the peak in the range of $(\frac{k_p}{2}, k_{max})$ or $(k_p * \frac{2}{3}, k_{max})$. An example of a worse case scenario is, when k_p is 0.058rad/m and H_s is 1m, we search for the peak from the 4 adjacent points of k_p.

G. Directional function and directional spread

It is known that the directional function and the associated directional spread vary with the wave number k ([18], [19]) . Here the emphasis is put on the directional function and the directional spread at the peak frequency (or peak wavenumber). According to (9) the directional function for the SWIM spectra, $D_{Swim}(k_{p_Swim}, \phi)$ can be obtained by:

$$D_{Swim}(k_{p_Swim}, \phi) = \frac{k_{p_Swim} \cdot F_{Swim}(k_{p_Swim}, \phi)}{F_{Swim}(k_{p_Swim})} \quad (22)$$

where k_{p_Swim} is the peak wavenumber provided by SWIM L2 data products, $\phi = 15° * (M-1)$, (hereinafter referred to as $\phi(M)$) , M =1,2…12. For buoy, $D_{Buoy}(k_{p_Buoy}, \phi)$ are obtained with a similar expression, from the directional spectra estimated with the MEM method, where here ϕ is a continous variable. For a subclass list in Table 1, the mean directional function $\overline{D}_{Swim}(k_{p_swim}, \phi(M))$ is calculated by averaging all $D_{Swim}(k_{p_Swim}, \phi(M))$ samples for the subclass, while $\overline{D}_{Buoy}(k_{p_Buoy}, \phi)$ is calculated by averaging all $D_{Buoy}(k_{p_Buoy}, \phi)$ samples.

However, $\overline{D}_{Buoy}(k_{p_Buoy}, \phi)$ from buoy measurement cannot be compared directly with $\overline{D}_{swim}(k_{p_swim}, \phi(M))$. This is because when using the MEM method, the azimuth discretization of $F(k,\phi)$ for a buoy sample can be chosen arbitrarily, while that of a SWIM spectrum from the L2 product is 15°. According to the processing method for L2 data, in fact, $F_{Swim}(k,\phi)$ at each azimuth bin of 15° is an average of at least two L1B consecutive observations with an azimuth interval of about 7.5° (here the case of three observations is ignored). Based on this fact, we need establish the statistical model of $\overline{D}_{swim}(k_{p_swim}, \phi(M))$, and then derive the formula for calculating the corresponding $\overline{D'}_{Buoy}(k_{p_{Buoy}}, \phi(M))$. The method to obtain $D'_{Buoy}(k_{p_{Buoy}}, \phi(M))$ is detailed in the Appendix.

It is recalled here that the wave height spectrum provided in the SWIM products contains a 180° ambiguity. Therefore, the results of the buoy data are also analyzed with this 180° ambiguity.

In the following, the directional function $\overline{D}_{swim}(k_{p_swim}, \phi(M))$ is compared with $\overline{D'}_{Buoy}(k_{p_Buoy}, \phi(M))$, where ϕ is given in 12 bins of 15° in the range (0,180°) and $\phi(M) = 0$ (i.e. $M = 1$) indicates the observation azimuth bin along the wave direction.

Now, based on the directional function $\overline{D}_{swim}(k_{p_swim}, \phi(M))$ and $\overline{D'}_{Buoy}(k_{p_Buoy}, \phi(M))$ we can calculate the directional spread $\Delta\phi_{buoy}(k_{p_Buoy})$ and $\Delta\phi_{swim}(k_{p_swim})$ for buoy and SWIM data, respectively, according to the following equation (dropping the wavenumber k_{p_Buoy} *or* k_{p_swim}).

$$\Delta\phi_\alpha = \sqrt{\sum_{M=1}^{12}(\phi(M) - \overline{\phi_{0_\alpha}})^2 \cdot \overline{D}_\alpha(\phi(M)) \cdot d\phi} \quad (23)$$

$$\overline{\phi_{0_\alpha}} = \arctan\left(\frac{b_{1_\alpha}}{a_{1_\alpha}}\right) \quad (24)$$

$$a_{1_\alpha} = \sum_{M=1}^{12} \cos(\phi(M)) \cdot \overline{D}_\alpha(\phi(M)) \cdot d\phi \quad (25)$$

$$b_{1_\alpha} = \sum_{M=1}^{12} \sin(\phi(M)) \cdot \overline{D}_\alpha(\phi(M)) \cdot d\phi \quad (26)$$

Where α denotes buoy and SWIM, respectively, $d\phi = 15°$ .The calculation of a_1 and b_1 with (25) and (26) is equivalent to that resulting from Eq. (16) of [26] based on the co- and cross- spectra of temporal series. In section III, the SWIM directional spread $\Delta\phi_{swim}$ will be compared with $\Delta\phi_{buoy}$ by buoy measurements for the different wind and sea surface conditions.

H. Spectral evaluation indexes

The linear (Bravais-Pearson) correlation coefficient ρ is defined as a metrics to analyze the similarity of the measurement spectrum and the reference spectrum in the comparison, which is the average of measurement samples and reference samples, respectively.

$$\rho(A,B) = \frac{\sum_{i=1}^{N}(A_i-\mu_A)(B_i-\mu_B)}{\sqrt{(\sum_{i=1}^{N}(A_i-\mu_A)^2)(\sum_{i=1}^{N}(B_i-\mu_B)^2)}} \quad (27)$$

Where A_i and B_i are respectively the mean SWIM and the mean reference buoy spectra discretized on wave numbers k_i (i =1,…N). As described in section II-B, k_i is with a wavenumber interval of $\Delta k = 0.0002$ over the wavenumber range $(0.0126, 0.28)$. μ_A and μ_B are the mean value of A_i and B_i, respectively. For example, for the omni-directional spectrum comparison, A_i and B_i in (27) are $F_{Swim}(k_i)$ and $F_{Buoy}(k_i)$, respectively.

> <

In order to quantitatively evaluate the difference between the SWIM spectrum and the reference buoy spectrum, the relative integral error ΔE is defined as:

$$\Delta E = \frac{\sum_{i=1}^{N} A_i \Delta k_{Ai} - \sum_{i=1}^{N} B_i \Delta k_{Bi}}{\sum_{i=1}^{N} B_i \Delta k_{Bi}} \times 100\% \quad (28)$$

The summation operation in (27) and (28) is carried out in the wave number range of (k_{min}, k_{max}).

In order to estimate the difference of peak wave number between the SWIM spectrum and the reference buoy spectrum, the peak wave number error Δk_{p1} is defined

$$\Delta k_{p1} = \frac{k_{p1_A} - k_{p1_B}}{k_{p1_B}} \times 100\% \quad (29)$$

Where k_{p1_A}, k_{p1_B} are the wave number at which the SWIM spectrum, and the reference spectrum are maximum, respectively. It is noted k_{p1} is different from the peak wave number k_p in Table 1.

III. Comparison of Omni-Directional Wave Height Spectra

After applying the data processing described above, including the wavenumber interpolation, the Tukey's test on the integral value of each spectrum sample, and the spectrum average in normalized wavenumber bins, we obtain the averaged omnidirectional wave height spectrum measured by SWIM and buoy under the different sea state conditions defined in Table 1 from the matched SWIM and buoy data sets. In this section, the averaged omnidirectional wave height spectrum from SWIM is compared with that from buoy for wind wave and swell conditions, respectively.

A. Wind wave conditions

Omni-directional wave height spectra $F_{Swim}(k)$ from SWIM spectra (estimated as explained in section II-D) are compared to their NDBC buoy counterpart $F_{Buoy}(k)$ in Fig. 2 for developing waves (Fig. 2 a-b-c-d-e-f), mature waves (Fig.2 g-h-i) and fully developed waves (Fig.2 j-k-l). Fig. 2 (a-d-g-j), (b-e-h-k), (c-f-i-l) correspond to the results for the 6°, 8°, 10° beams of SWIM respectively.

Fig.2(a-b-c-d-e-f) illustrate comparisons for $F(k)$ in the selected cases of developing sea wave (Ω = 1.3) with wind speed 12, 14, 16, 18, 20m/s. The solid lines in the figures represent $F_{Swim}(k)$, the dotted dots represent $F_{Buoy}(k)$, and the number of samples corresponding to each spectrum line is marked in the legend (and also reported in Table 1) . Wave steepness corresponding to each sea surface condition $\delta = H_s/\lambda_p$, and the evaluation indexes $\rho, \Delta E$ and Δk_{p_1} of each omni-directional spectrum from SWIM, relative to those from buoy data, are also indicated in the legend. The results for all wind waves conditions will be discussed further down with Fig 3.

For the conditions of young developing wind waves and wind speed no more than 14 m/s, (corresponding to $H_s = 2.5m$), it appears that the SWIM 6° beam wave spectra are quite different from those of the buoy and its correlation coefficient is relatively low, the spectral values measured by the SWIM near the peak are all less than those from the buoy, the peak wave number is shifted to the left relative to the peak wave number of the buoy and a parasitic peak is present at low wavenumbers. Clearly these are conditions where SWIM 6° beam is not able to provide correct wave spectra. The discussion at the end of section III-A proposes some reasons for that. In opposite, for larger wind speeds of 16, 18 and m/s, under developing wind waves conditions, the correlation coefficient ρ between SWIM and buoy spectra is between 0.76 and 0.99 and the leftward shift of the peak number is small for all beams, ΔE is less than 20% (equivalent to a H_s error less than 10%) for SWIM beams 8° and 10°. So in these young wave conditions under high wind speeds, SWIM seems able to provide correct spectral information, even if an overestimation of energy at small wavenumbers is still apparent.

For mature wind waves (Fig.2 (g-h-i)), whatever is the SWIM beam, the correlation coefficient is close to or larger than 0.90). Correlatively in the same conditions, the absolute relative bias in energy is less than 20% (or close to 20%), and the relative error on k_{p1} remains under 10% for all SWIM beams. Compared to the young sea cases, the better agreement with buoy spectra is mainly due to the weaker impact of the parasitic peak.

For fully developed wave conditions (Fig.2 (j-k-l)), the correlation coefficient is larger than 0.90 for all conditions displayed in the figure, except for spectra of SWIM 6° beam where this 0.90 value is reached only if the wind speed is larger than 14 m/s ($H_s \geq 4.6$ m). The absolute value of the relative bias in energy is less than 20% for all displayed cases (wind speed of at least 12 m/s). Fig.2(j-k-l) show that the parasitic peak at low wave number still contributes to the bias for the smallest values of wind speed). The relative bias in k_{p1}remains under 10%). Overall, for these cases with wind speed above 12 m/s and similarly to the case of mature sea conditions, we find a good agreement between SWIM and buoy spectra for all the SWIM beams.

> <

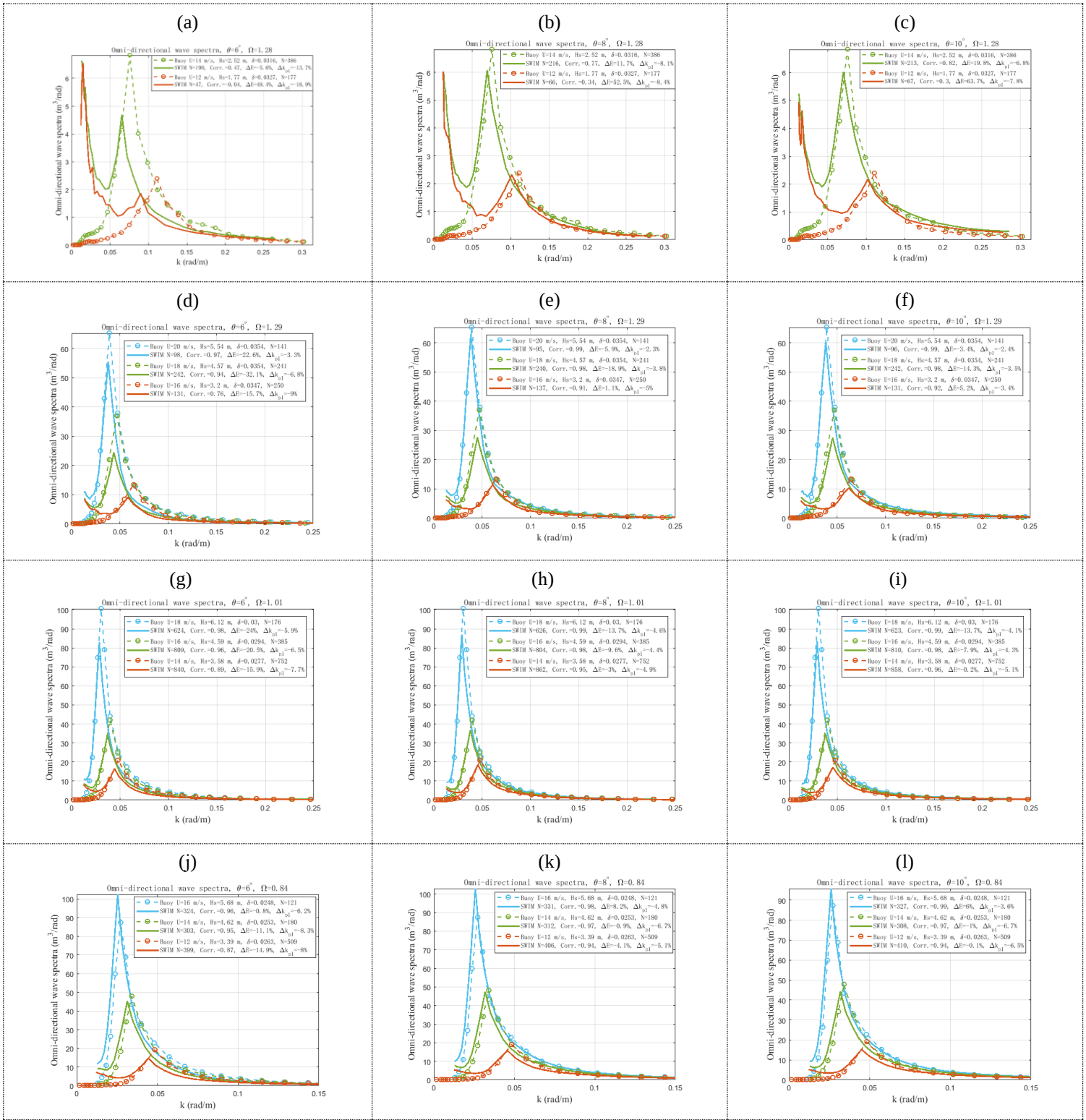


Fig. 2. Comparison of omni-directional wave height spectra from SWIM and buoy for wind wave sea under developing conditions $\Omega = 1.3$ (a-b-c-d-e-f), mature conditions $\Omega = 1.0$ (g-h-i), and fully developed conditions $\Omega = 0.84$ (j-k-l). The wind conditions are 12 m/s(red) and 14 m/s (green) for Fig. 2 (a-c) , 16 m/s (red), 18 m/s(green) and 20 m/s (cyan) for Fig.2(d-f) ,14 m/s (red), 16 m/s(green) and 18 m/s (cyan) for Fig.2(a-f) , whereas they are 12 m/s (red), 14 m/s (green) and 16 m/s (cyan) in Fig.2(g-i). Results are shown for the SWIM beam 6° (a-c-g-j), 8° (b-d-h-k), and 10° (c-f-i-l)

More generally, the consistency of SWIM spectra compared to buoy data increases with incidence angle and with the wave height. This is illustrated in Fig.3 which show, as a function of H_s, the coefficient ρ (absolute value), the relative bias in energy (ΔE) and in k_{p1} (Δk_{p1}) for all SWIM beams and for all the wind wave conditions listed in Table 1. Clearly,

SWIM beams at 8° and 10° provide consistent information ($\rho \geqslant 0.80$, $\Delta E \leq 20\%$, $\Delta k_{p1} \leq 10\%$) only when H_s is larger than about 2.5 m. The performance for beam 6° is significantly less with these scores reached only when H_s is larger than about 3.2 to 3.5 m. We also studied the variation of these score indexes with the significant slope δ. This is illustrated in Fig.4 where the different symbols distinguish the different incident beams, and the different colors distinguish the different wind speeds. It is noted that for the sake of clarity, to avoid discussing trends due to effect of the parasitic peak on ΔE, only the cases the less affected by the parasitic peak are plotted in Fig.4(b). From Fig.4(a-b), it is seen that ρ decreases, and the absolute values of ΔE increases with δ under the same wind speed. It is found that for a given SWIM beam the absolute values of ΔE tend to be larger for the 2 largest slope values (δ=0.030 and 0.036), and are larger for the SWIM beam 6° than for beams at 8° and 10°. Correlatively, Fig.4(c), shows that the absolute value of Δk_{p1} depends on δ and wind speed, showing a complex nonlinear relationship with them, and is always the largest for the SWIM beam 6°.

In these wind-wave conditions, three factors may explain the relative low consistency between SWIM spectra (processed as here with the MTF1 modulation transfer function) and buoy data. First, whatever is the SWIM beam, when the wave energy is small, a parasitic peak (not related to waves) is evidenced at small wavenumbers. The energy of this peak contributes significantly to the energy bias and may also impact the estimation of the peak of spectrum. This parasitic peak is likely due to remaining energy associated to either heterogeneity of the sea surface [4] or residual speckle energy which is amplified at low wave numbers when converting wave slope spectrum to wave height spectra by dividing by the square of the wave number (see also [4], or [14]). As illustrated in Fig.2, this effect is relatively similar for the three beams but its impact on the energy bias and on the correlation coefficient clearly decreases when the significant wave height increases. For high wave heights, such a non-wave signal in the lower wave number part of $F_{Swim}(k)$ still exists, but does not affect too much the comparison with the buoy spectrum since it is much weaker than the wave signal. Overall, the wind-wave omni-directional wave height spectra from SWIM are significantly affected by the parasitic peak problem (meaning with energy in this peak higher that the real peak due to waves) when H_s < 2.3 to 2.5m (depending on the wave age). This indicates the need to correct the wave spectra from this problem when converting wave slope to 1D wave height spectra.

However, even when ignoring this parasitic peak, another effect is obvious, in particular for the smaller incidence angle and/or the less developed wind waves: the peak of the wave energy containing part is shifted towards the low wavenumbers compared to the buoy spectrum and is less energetic for SWIM than for buoy (see for example Fig.2(a-b), and Fig.3-4). This phenomenon is mainly caused by the surfboard effect as suggested by the study of [23] This is due to the following geometric effect. When the angle of incidence is smaller than the wave slope (i.e., for incidence angles of a few degrees, depending on sea state) the iso-range plane cuts the rough surface at multiple points, like a long surfboard in choppy seas. This non-linear sampling effect is called surfboard sampling, and is relevant for the near-nadir radar systems. As shown by Fig.5(d) of [3], it can be predicted from simulations that this surfboard effect is exacerbated when the radar incidence angle becomes smaller or the sea wave becomes steeper. It can be seen from the results of various subgraphs in Fig.2 (and this is true also on the other cases which are not illustrated) that indeed the absolute biases in energy and peak wavenumber decrease with wave age, and for a given wave age decrease with incidence angle. Fig.3 and 4 confirm that these biases in energy and peak wavenumber increase with the significant slope, which tends to confirm that these biases are due to the surfboard effect.

The third effects which slightly degrades the coherence between SWIM and buoy spectra is observed in the high wavenumber part of the spectrum in certain conditions. In particular, in the cases of developing seas with wind speed of 12 m/s and 14 m/s, shown in Fig.2(c) indicates that the spectrum value at high wavenumbers is slightly larger than that of the buoy spectrum for SWIM beam 10°. This may be due to the underestimation of the speckle noise spectrum in such sea conditions and for these incidence beams.

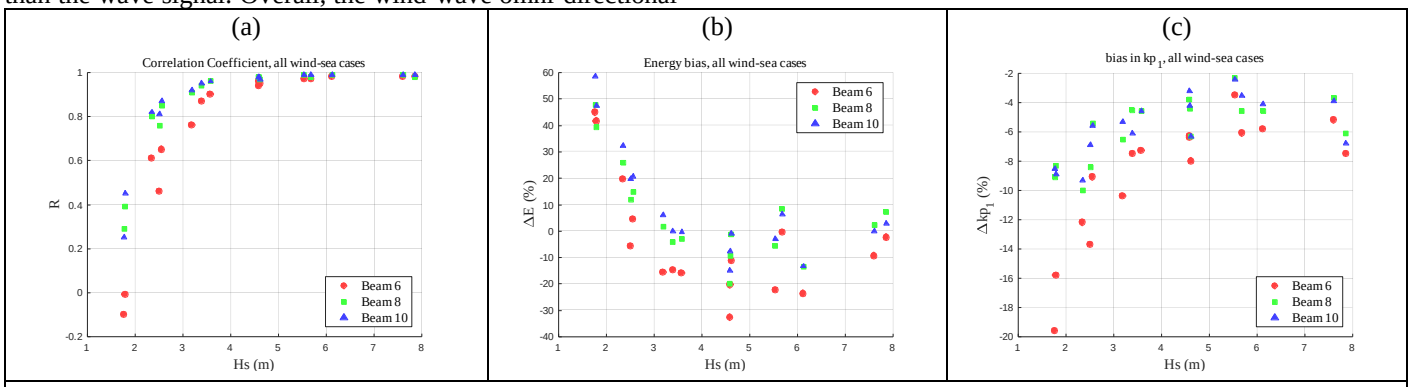


Fig.3. Correlation coefficient (a), relative bias in energy E (b), relative bias in peak wavenumber k_{p1} (c), as a function of significant wave height H_s for the SWIM spectra from the three beams (6° in red, 8° in green, 10° in blue symbols) compared to the buoy spectra, and for all the considered wind sea cases. see text and Table 1 for details.

> <

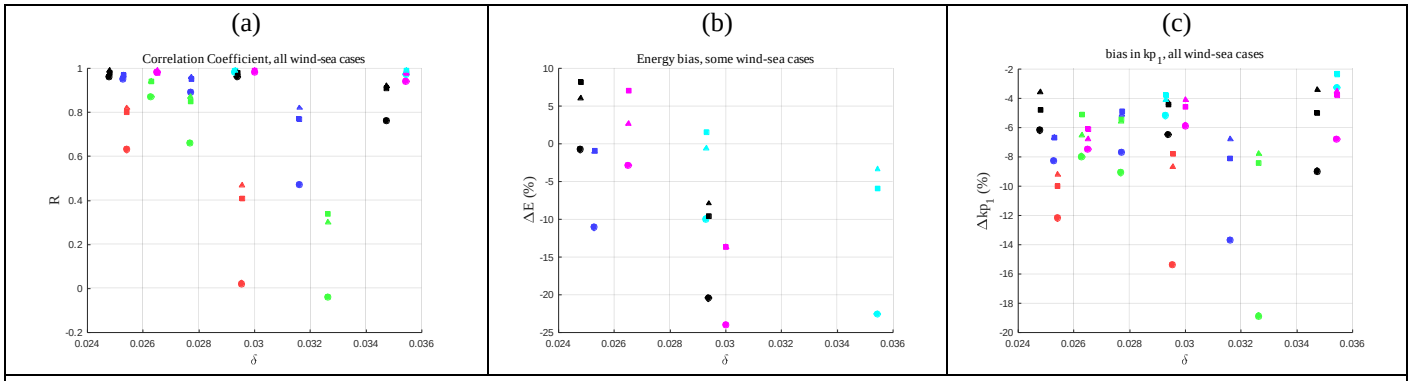


Fig. 4. Correlation coefficient (a), relative bias in energy E (b), relative bias in peak wavenumber k_{p1} (c) as a function of significant slope δ for the SWIM spectra from the three beams (6° with circles, 8° with squares, 10° triangles) compared to the buoy spectra, and for all the considered wind sea cases. Red, green, blue, black, magenta and cyan represent wind speeds ranging from 10m/s to 20m/s at intervals of 2m/s. In (b), only the cases less affected by the parasitic peak are plotted.

B. Swell conditions

Fig.4 shows the comparison of omni-directional wave height spectra of SWIM with the buoy measurements $F_{Buoy}(k)$ under swell conditions. The peak wavelengths and significant wave heights of the swell considered here are those recalled in Table 1. Fig.5 shows a selection of results corresponding swell with peak wave numbers from 0.0308 down to 0.0157 rad/m

The parasitic peak at low wavenumber is not apparent in these cases, but still exists for the classes with k_p=0.0580 rad/m, H_s= 1, 2 and 2.5 m (not shown). In all other cases, this parasitic peak does not seem to impact significantly the spectrum at low wave number. This is confirmed by the correlation coefficient, which is larger than 0.9 in all the cases except the one mentioned above. It is remarkable that the correlation coefficient remains close to 1 for all SWIM beams and all swell cases with $H_s \geq 3$m.

However, some differences between the SWIM spectra compared to the buoy ones appear in certain conditions: for example, for the classes with k_p=0.0308 rad/m, H_S= 4 and 5 m (Fig.5(a-b-c)), the energy of the wave energy containing part is a little bit smaller for SWIM compared to that of the buoy. This is similar to what was discussed for developing waves in Section III-A. As this effect tends to be larger for larger significant slopes, it is likely that the surfboard effect can again be invoked to explain this slight underestimation of the SWIM energy density. When k_p =0.0157 (λ_p = 400 m) and H_s is between 3 and 6 m (see Fig.5(g-i)), it is seen that SWIM spectral maxima are slightly larger than those from the buoys. The reason for this slight difference is still unknown. We speculate that another nonlinear effect related to long wavelength may lead to this difference. However, this conjecture lacks theoretical basis at present. In order to truly understand this phenomenon, it is necessary to strengthen the research on the modulation spectrum model of spectrometer with not only linear tilt modulation, but also all kinds of nonlinear modulation taken into account.

> <

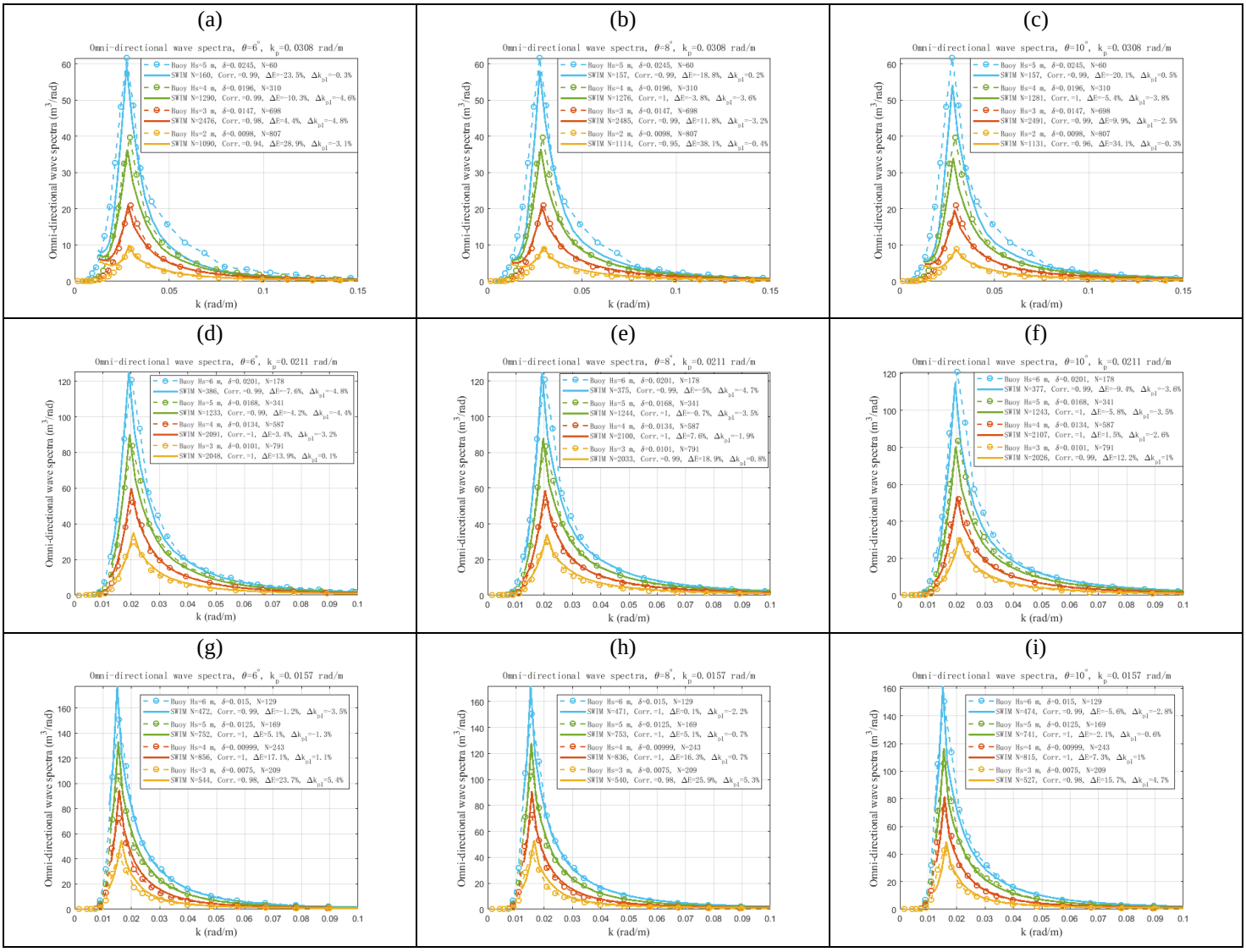


Fig. 5. Mean omni-directional wave height spectra from SWIM L2 data (solid lines) and buoys (dashed lines) for swell conditions. The comparisons are shown for the SWIM beams at 6° (a,d,g), 8° (b,e,h), and 10° (c,f,i). Panels a-b-c are for mean conditions with k_p=0.0308 and H_s= 2 m (yellow), 3 m (red), 4 m (green), and 5 m (cyan). Panels d-e-f are for k_p=0.0211 and H_s= 3 m (yellow), 4 m (red), 5 m (green), and 6 m (cyan). Panels g-h-i are for k_p=0.0157 and H_s= 3 m (yellow), 4 m (red), 5 m (green), and 6 m (cyan).

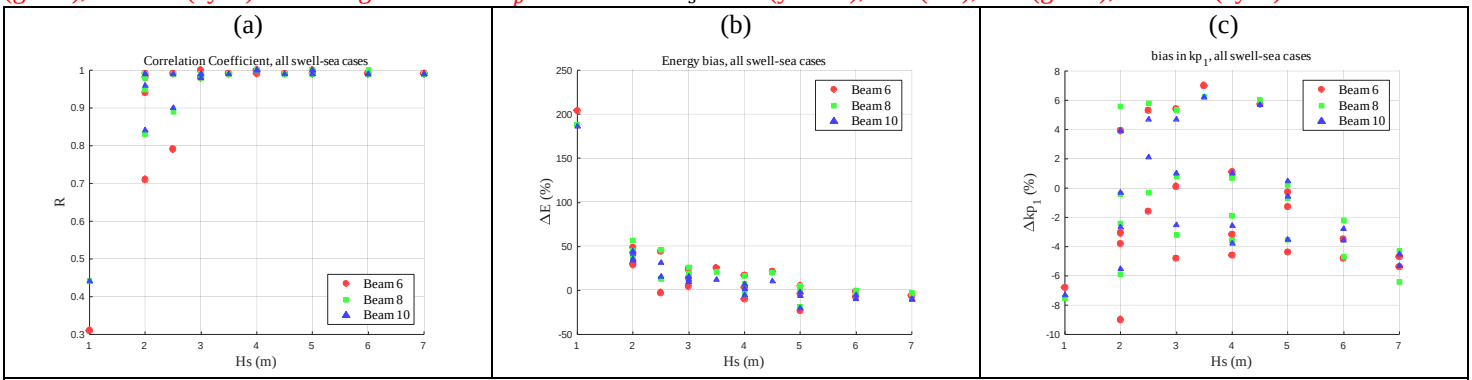


Fig. 6. Correlation coefficient (a), relative bias in energy E (b), relative bias in peak wavenumber k_{p1} (c), as a function of significant wave height H_s for the SWIM spectra from the three beams (6° in red, 8° in green, 10° in blue symbols) compared to the buoy spectra, and for all the considered swell cases. See text and Table 1 for details.

> <

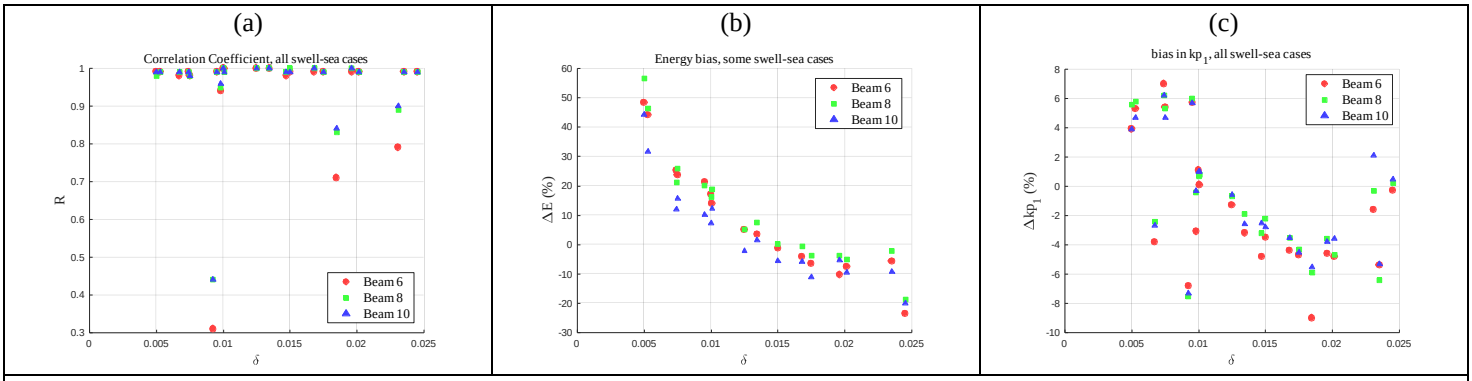


Fig. 7. Same parameters as in Fig. 6 but plotted as a function of the significant slope δ. Here, only the cases slightly influenced by the parasitic peak are shown.

The correlation coefficient, the bias on energy and wave numbers are shown in Fig.6 as a function of H_s for all the SWIM beams and all the swell sea conditions. This figure shows that for the smallest values of H_s (lower than 2-2.5 m), the correlation coefficient is generally low and the energy bias is positive and quite large, whatever is the SWIM beam. In these cases, the overestimation of energy is mainly due to the presence of the parasitic peak. Starting from about 3m in wave height, the energy bias remains close to the ± 20% interval (meaning an error of less than about 10% in H_s). It is interesting to note that for these swell cases with H_s above 3m, the performance of the 3 SWIM beams is almost similar. Concerning the peak wavenumber, we find that for all the SWIM beams, the relative bias in k_{p1} with respect to the buoy data always remains within the ±10% interval (after the parasitic peak is filtered out).

In order to study the influence of wave steepness on the comparison results, Fig.7 shows ρ, ΔE and Δk_{p1} as a function of significant slope δ. In order to eliminate the influence of pseudo peaks on the comparison results, those cases that are greatly affected by pseudo peaks have been removed from the graph. From Fig.7, it is clearly seen that the biases of both energy and peak wavenumber decrease from positive to negative with the increase of significant slope. This trend may indicate that a small nonlinearity effect exists in the detection of swell.

IV. Comparison of Directional function and directional spread

In this section we analyze the directional distribution of energy $D_{Swim}(k_{p_Swim}, \phi)$ and directional spread $\Delta\phi_{swim}(k_{p_Swim})$ at the peak wave number of SWIM spectra k_{p_Swim}, and compare it with its counterpart from buoy spectra (according to the method presented in Section II-H), $D_{Buoy}(k_{p_Buoy}, \phi)$ and $\Delta\phi_{buoy}(k_{p_Buoy})$ where ϕ is the observation angle relative to the dominate wave direction. In order to reduce the influence of parasitic peaks on the comparison results, the samples significantly affected by these parasitic peaks (low signal-to-noise ratio) have been excluded from the comparison.

A. Wind wave conditions

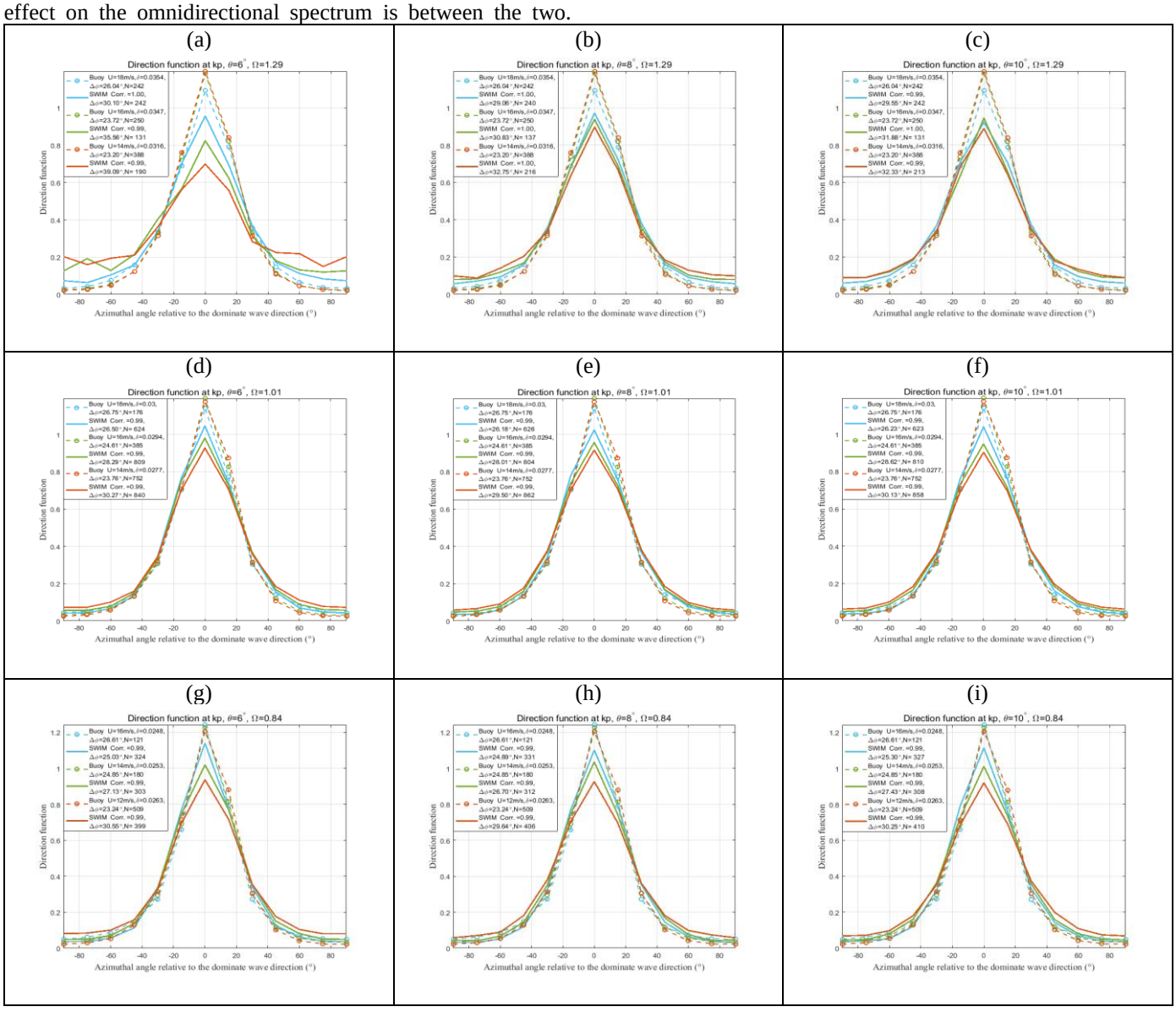
The comparison of the directional functions $D_{Swim}(k_{p_Swim}, \phi)$ and $D_{Buoy}(k_{p_Buoy}, \phi)$ are shown for some wind sea cases in Fig.8, for developing (Fig.8(a-c)), mature (Fig.8(d-f)) and fully developed (Fig.8 (g-i)) wind waves, respectively. The directional spread $\Delta\phi$ is denoted in the legends.

For all wind wave conditions, it can be seen from Fig. 8, that both the buoy and the SWIM directional functions show a symmetric distribution around the 0 ° azimuth. The results are consistent for the three SWIM beams and show that even if some differences exist in the details of the directional function, there is a high consistency of the directional function of the SWIM spectra compared to the buoy spectra, as indicated by the high correlation coefficients relating both (all above 0.98). For the three beams of SWIM, when the azimuth is close to 0°, i.e., observing along the dominant wave direction, the directional function of SWIM is smaller than that of the buoy except for the fully developed wind sea when wind speed is 18 m/s. In opposite, for directions far from the dominant directions (directions separated by more than 40° to 50°), the directional function values for SWIM are significantly larger than those from buoy for the young wind-sea conditions (all wind cases) and for the mature and fully-developed wind sea cases when the wind is less or equal to 14 m/s. We discuss further below this double feature of the directional function (underestimation with respect to the buoy spectra in the wave direction, overestimation away from the wave direction).

Fig.9 shows the variation for the directional spread with the wave age (Fig. 9(a)) for the SWIM beam 6 ° (circle), 8° (square), 10° (triangles) and the buoy data sets (stars), where the yellowish triangles refer to the results for swell conditions, and all other colored triangles represent the results for wind wave conditions with the same color code as in Fig .4. From Fig. 9(a), it is seen that there is no apparent differences in buoy directional spreads between SWIM and buoy directional functions for wind wave cases. Also, there is no obvious trend between buoy directional spread and the inverse wave age. However, it is seen that the directional spreads for all the SWIM beams increase with the inverse wave age for the same wind speed. This is in agreement with the findings of [18] or [22]

based on buoy observations in fetch limited conditions, and also with the results of [5] based on SWIM data in the Southern Ocean.

The differences between SWIM and buoy directional spread are shown in Fig.9(b) as a function of the inverse wave age. From Fig.9(b), it is seen that the differences for the swell conditions are between -7° and +7° (to be analyzed in IV-B in details). The range of spread bias for wind waves is about $-3°\sim+12°$ for beams 6° and $-3°\sim+8$ for beam 8° and 10°. Almost all the bias for the SWIM beam 6°are larger than those for beam 8° and 10°. The bias for the wind sea cases increase with the inverse wave age. We consider that this result is caused by the surfboard effect on the directional function from SWIM. As mentioned in Section III-A, at the same wind speed, the surfboard effect is more significant with the increase of the inverse wave age. Obviously, the surfboard effect is the largest along the wave direction and the smallest in the side wave direction, while the surfboard effect on the omnidirectional spectrum is between the two. According to the definition formula of direction function (22), it will lead to the smaller value of the directional function of SWIM spectra along the wave direction and the larger value of the direction function away from this direction. Furthermore, according to the definition of the directional spread (23), the value of the directional function away from the mean wave direction has a decisive effect on the directional spread, i. e., the larger value of the direction function in directions away from the dominant direction causes the directional spread to be overestimated compared to estimates from buoy data. It is worthwhile to note that the three cases with a directional spread bias greater than 10° (red, green and black circles), correspond to SWIM beam 6° for wind sea with low to medium wind speeds. These are also the cases where the difference in energy far from the peak is the most visible, while in the same cases, the surfboard effect is also the most significant as shown in Fig.2.



> <

Fig.8. Comparison of the directional function at the peak wavenumber from the SWIM (solid lines) and the buoy measurements (dashed lines), for the wind wave cases. The different colors refer to different wind speeds (same color codes as Fig.2). Fig.8(a-b-c), (d-e-f), (g-h-i) are respectively for young wind waves (inverse wage age $\Omega = 1.29$), mature wind waves ($\Omega = 1.00$) and fully developed wind waves ($\Omega = 0.84$), respectively. For SWIM, the results are shown for the beam 6°(a,d,g) , 8°(b,e,h) and 10°(c,f,i)

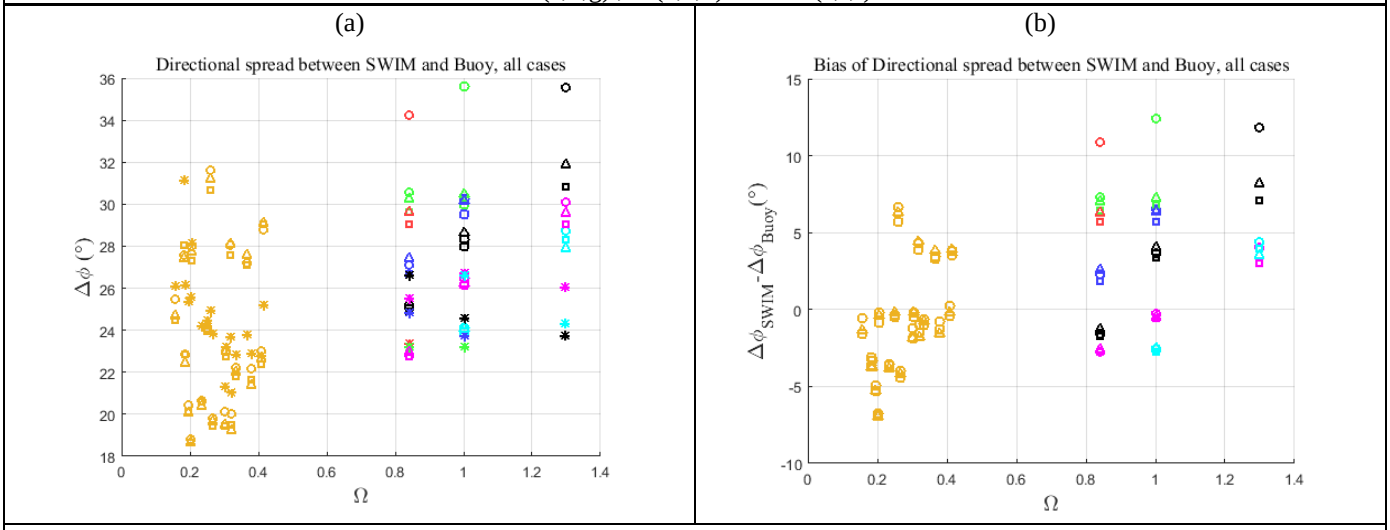


Fig.9. Directional spread from the buoy data set (stars) and SWIM beam 6° (circle), 8°(square), 10° (triangle)as a function of the significant slope (a), difference in the directional spread as a function of the significant slope (b). The meanings of colors are as the same as those in Fig.7.

B. Swell conditions

Fig.10 shows comparison of directional function comparisons from SWIM $D_{Swim}\left(k_{p_Swim}, \phi(M)\right)$ and buoy $\overline{D'}_{Buoy}\left(k_{p_{Buoy}}, \phi(M)\right)$ for some swell sea cases with different H_s when k_p=0.0308 (Fig.10(a-c)), k_p=0.0211 (Fig.10(d-f)) and k_p=0.0157 (Fig.10(g-i)). First, it can be noted that the correlation coefficients between buoy and SWIM directional function is more than 0.98 for all the considered swell cases and all the SWIM beams. It is seen from Fig.10 that for the cases of relatively short peak wavelengths (k_p=0.0308 $i.e\ \lambda_p$ =204 m), the directional function values in the dominant wave direction from all the SWIM beams are all smaller than those from the buoy spectra, while far away from the wave direction, the directional function from SWIM is larger than that from the buoys. The above phenomenon occurs when the wave steepness is equal or greater than about 0.01, thus this inconsistency with buoy is also partly related to the surfboard effect (see Fig.5(a-c) for their corresponding omni-directional spectra). In opposite, for the case with $k_p = 0.0157$ ($\lambda_p = 400$ m) and H_s=3 m (yellow curves), it is seen that directional function values from SWIM in the dominant wave direction is larger than that from the buoy data set, while away from the wave direction, the directional function from SWIM is smaller than that from the buoys. As previously analyzed, the direction function value away from the wave direction partly determines the direction expansion. Therefore, the underestimate of the direction function value away from the dominant wave direction leads to the fact that the SWIM directional spreads are lower than those of the buoy. It is noted that this phenomenon occurs only when the wave steepness is smaller than 0.01. As we explained for Fig.5, under this sea surface condition there may exist another nonlinear effect related to long wavelength, which result in that the omnidirectional spectrum of SWIM (Fig.5(g-i)) is larger than that of the buoy.

The variation of the directional spread with the inverse wave age Ω for the same significant wave height is shown in Fig.11(a) for swell conditions with different color for different the significant height H_s. Stars, circles, squares and triangles correspond to the results from buoys, SWIM 6°, 8° and 10° beams respectively. From Fig.11(a), for swell conditions the relationships between the directional spreads from buoys and the inverse wave age Ω are not clear. The difference of the spreads for the swell conditions are shown in Fig.11(b). From Fig.11(b), the difference of spread for the swell conditions increases with the inverse wave age for a given significant height, with the range of the spread bias of $-7° - +7°$ (about -4° to +4° for 80% cases here). Most bias for the swell conditions are negative. In the study [24] it was shown that the directional spread of NDBC buoy may be overestimated by about 4° [24, Fig.6] under swell conditions. So part of the systematic difference may be explained by this fact. However, due to the above-mentioned nonlinear effect for SWIM, the direction function value away from the wave direction is less than the buoy value (see Fig.10(g-i)), which leads to the underestimation of the directional spreads. However, when the wave steepness is greater than about 0.01 and the significant wave height is smaller than about 4 m, due to the surfboard effects, the direction function value away from the wave direction is greater than the buoy value, which makes the directional spread difference positive in this case. In addition,

> <

from Fig.11(b), we find that the bias of directional spread are also not related to the incidence beam for swell conditions.

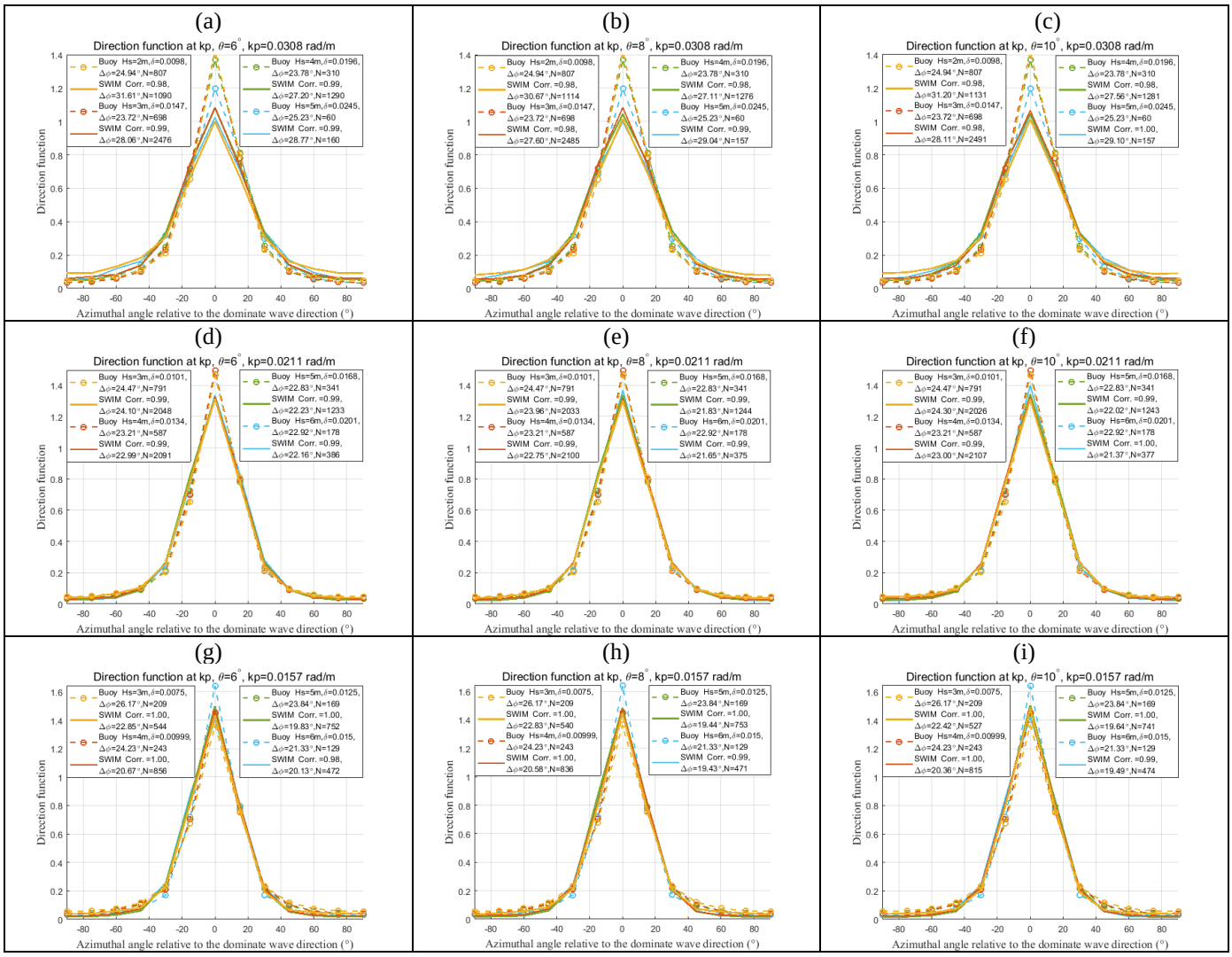
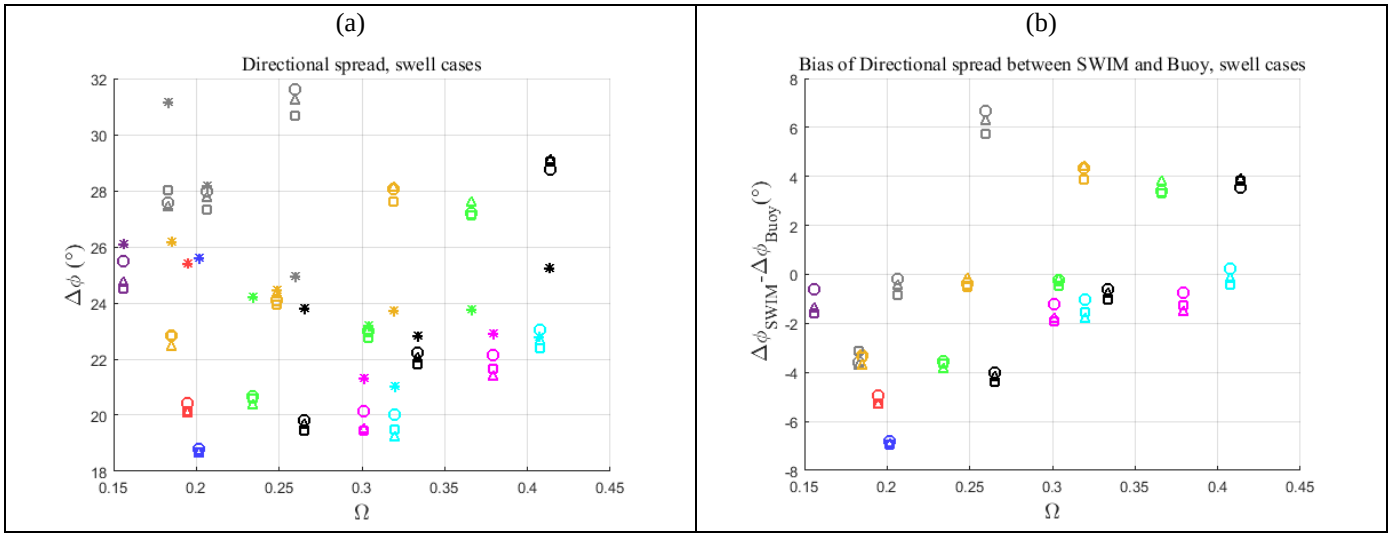


Fig. 10. Comparison of directional function by SWIM and Buoy measurements, for swell sea, a,b,c for k_p=0.0308, H_s=2 m, 3 m, 4 m, 5 m; d,e,f: for k_p=0.0211, H_s=3 m, 4 m, 5 m ,6 m ; g,h,i: for k_p=0.0157, H_s=3 m, 4 m, 5 m ,6 m. ..



> <

Fig. 11. Directional spreads from the buoy data set and SWIM beams for swell conditions, as a function of the inverse wave age (a), difference of the directional spread as a function of the inverse wave age (b). Gray, purple, yellow, red, green, blue, black, magenta and cyan correspond to the significant height of 2m, 2.5m, 3m, 3.5m, 4m, 4.5m, 5m, 6m and 7m respectively. Stars, circles, squares and triangles correspond to the results from buoys, SWIM 6 °, 8 ° and 10 ° beams respectively.

V. Conclusion

For wave spectra provided from SWIM observations acquired on-board the CFOSAT satellite, several validation studies have been proposed in the past [4]–[7], but they were mainly concentrated on the main parameters (such as significant wave height, peak frequency, peak direction) and the performances were not detailed according to the sea state conditions. Some studies were also devoted to the shape of the SWIM spectra as in [5] but the main part of the comparison was done with model data as reference.

In this paper we concentrate on the spectral analysis by comparing spectra provided by the SWIM instrument, with buoy spectra. Because of the difficulty to gather a large statistics of time-space matching pairs, and also to better define the optimal conditions where we can be confident in the SWIM data, we developed a comparison method based on mean spectra estimated for different classes of sea state conditions. By defining for both SWIM and buoy the same sea state classes (wind wave/ swell) and sea surface classes (wind speed, peak wave number and significant wave height), we compare the statistical characteristics of the wave spectra obtained from the two data bases (2 years of NDBC buoy, two month of SWIM data at the global scale). Model data from the MFWAM model were used in complement to define the wind sea and swell classes and to screen out the situation where a single wave component is dominant.

We analyzed the directional wave height spectra provided by SWIM in the option where the Modulation Transfer Function (relating signal modulation to wave slopes) is not constrained by the significant wave height provided by the nadir altimeter beam. We compared the SWIM spectra provided by the 3 different beams of SWIM (from incidences 6°, 8°, 10°) with the buoy wave directional spectra, under different sea states and sea surface conditions (10m/s≤U≤20m / s, 1m≤H_s≤7m) and discussed the results for the omni-directional weight height spectra and the directional function at the peak wave number.

Our results show that:

For wind wave conditions, SWIM data from beams 8° and 10° provide omni-directional spectra in good agreement with buoy data as long as the significant wave height is larger than about 2.5 m (corresponding to wind speed larger than about 12 m/s). In these cases the shape of the spectra are similar between the SWIM and the buoy data sets as indicated by the correlation coefficient which is close to or higher than 0.90, the relative bias on energy ΔE is within ± 20%, and the bias on the peak wave number Δk_{p1} is within ±10%. For the same wave conditions, the results are not as good for the beam 6° where similar scores are reached only for H_s > 3.5m and significant slope δ< 0.03. This difference between beam 6° and beams 8° and 10° is mainly due to the surfboard effect caused by a non-linear imaging mechanism in conditions of low incidence and high significant slope [3], [23].

At significant wave height less than about 2.5 m (or wind speed less than about 12 m/s), other factors explain the difficulty to estimate consistent wave spectra whatever is the SWIM spectral beam. The main one is the presence of a parasitic peak at low wave number which is due to the amplification of a noise floor of low energy remaining in the SWIM slope spectra but significantly amplified when these are converted to wave height spectra. Another factor but which only impacts marginally the consistency between buoy and SWIM spectra is the likely underestimation of speckle correction in certain conditions (mainly with relatively smaller H_s and larger peak wavenumbers).

In swell conditions, SWIM data from beams 8° and 10° provide omni-directional spectra and spectra in the dominant direction in good agreement with buoy data as long as the significant wave height is larger than about 2.5 m. The results also show that compared to buoy the SWIM beam 6° induces larger errors than the 8° and 10° beams, for the omni-directional spectra, in particular for swell with small H_s and large peak wavenumber. While for long wave length (such as 472m), it is seen that SWIM spectral maxima are slightly larger than those from the buoys, and the peak wavenumber from SWIM is shifted a little to the right relative to the peak wave number of the buoy, which is consistent with the results in [4]. However, this difference is small with ΔE within 20%, and the bias on the peak wave number Δk_{p1} within 7%. The reason for the phenomenon is not clear at present.

Overall, it is rather positive that the surfboard effect only affects SWIM data at low wind/wave conditions and mainly for the SWIM beam 6°. The two other perturbation effects (parasitic peak and small overestimation of speckle noise) should be reduced in the future with improved SWIM data processing schemes.

The directional functions from SWIM and from buoy are in good agreement with the correlation coefficient greater than or equal to 0.98. Due to the surfboard effect which occurs in certain conditions, the direction function value away from the wave direction is larger than the buoy value, which leads to the overestimation of the directional spreads up to 8° for SWIM beam 8° and 10°. The more significant the surfboard effect is, the more obvious the overestimation is, such as for the wind wave conditions with low to medium wind speed for SWIM beam 6°. On the contrary, for the sea surface conditions with the significant slope smaller than 0.01, where the surfboard effect is negligible and another above-mentioned nonlinear effect appears, the SWIM direction function value away from the wave direction is less than the buoy value, which leads to the underestimation of SWIM directional spreads. It is also noted that the overestimation of NDBC buoy spreads of about 5° [24, Fig.6] exist under swell conditions. The two later factors

together result in a spread bias of SWIM up to -7° for all the sea surface conditions included in this work.

Our study results on directional spread are based SWIM wave spectra provided with an angular discretization of 15°, and with buoy spectra derived from the MEM method with the same discretization. Although in our analysis we have somehow taken into account the higher original sampling of SWIM observations (~7.5°), it may be interesting in the future to extend the present analysis to SWIM spectra analyzed directly at the 7.5° discretization.

APPENDIX: BUOY DIRECTIONAL FUNCTION $\bar{D}_{Buoy}\left(k_{p_Buoy}, \phi(M)\right)$

Similarly to the approach presented in section 2.7, it is assumed that ϕ_p^n is just in an azimuth bin $(\phi_L^n, \phi_L^n + 15°)$ for a SWIM sample of the L2 product, and that in each azimuth bin $(\phi_A^n(M), \phi_A^n(M) + 15°)$, $\phi_A^n(M) = 15° * (\mathrm{M} - 1) + \phi_L^n, \mathrm{M} = 1, \ldots 12$ of that SWIM sample, there are two consecutive observations at the azimuth $\phi_1^n(M)$ and $\phi_2^n(M)$, where $\phi_1^n(M) - \phi_2^n(M) = 7.5°$. It is assumed that for all SWIM samples $\phi_p(M) - \phi_L$ is evenly distributed in the range of $(0°, 15°)$, $\phi_2(M) - \phi_L$ is evenly distributed in the range of $(\phi_B(M), \phi_B(M) + 7.5°)$ and $\phi_1(M) - \phi_L$ is evenly distributed in the range of $(\phi_B(M) + 7.5°, \phi_B(M) + 15°)$, where $\phi_B(M) = \phi_A(M) - \phi_L = 15° * (\mathrm{M} - 1), \mathrm{M} = 1, \ldots 12$. then we derive that

$$\phi_1(M) - \phi_{p_swim} \in (\phi_B(M) - 7.5°, \phi_B(M) + 15°) = (15° * \mathrm{M} - 22.5°, 15° * \mathrm{M}), \text{evenly distributed} \quad (30a)$$

$$\phi_2(M) - \phi_{p_swim} \in (\phi_B(M) - 15°, \phi_B(M) + 7.5°) = (15° * \mathrm{M} - 30°, 15° * \mathrm{M} - 7.5°), \text{evenly distributed} \quad (30b)$$

We then define $\phi_1(M) - \phi_{p_swim}$ as $d\phi_1(M)$, $\phi_2(M) - \phi_{p_swim}$ as $d\phi_2(M)$. So, the averaged directional function of all SWIM samples in the azimuth bin $(\phi_A(M), \phi_A(M) + 15°)$ can be approximated by:

$$\begin{aligned}\bar{D}_{swim}\left(k_{p_swim}, \phi(M)\right) &= 0.5 * \frac{1}{N}\sum_{n=1}^{N}\left[D_{swim}^n\left(k, \phi_1^n(M)\right) + D_{swim}^n\left(k, \phi_2^n(M)\right)\right] \\ &\approx 0.5 * \frac{1}{N}\sum_{n=1}^{N}\left[\bar{D}_{swim}\left(k, \phi_1^n(M)\right) + \bar{D}_{swim}\left(k, \phi_2^n(M)\right)\right] \\ &= 0.5 * < \bar{D}_{swim}\left(k_{p_swim}, \phi_{p_swim} + d\phi_1(M)\right) + \bar{D}_{swim}\left(k_{p_swim}, \phi_{p_swim} + d\phi_2(M)\right) > \end{aligned} \quad (31)$$

Correspondingly, the buoy averaged directional function counterpart to that of SWIM, is calculated by:

$$\bar{D}'_{Buoy}\left(k_{p_Buoy}, \phi(M)\right) = 0.5 * < \bar{D}_{Buoy}\left(k_{p_Buoy}, \phi_{p_Buoy} + d\phi_1(M)\right) + \bar{D}_{Buoy}\left(k_{p_Buoy}, \phi_{p_Buoy} + d\phi_2(M)\right) > \quad (32)$$

REFERENCES

[1] W. R. Alpers, D. B. Ross, and C. L. Rufenach, "On the detectability of ocean surface waves by real and synthetic aperture radar," *J. Geophys. Res.*, vol. 86, no. C7, p. 6481, 1981, doi: 10.1029/JC086iC07p06481.

[2] K. Hasselmann and S. Hasselmann, "On the nonlinear mapping of an ocean wave spectrum into a synthetic aperture radar image spectrum and its inversion," *J. Geophys. Res.*, vol. 96, no. C6, p. 10713, Nov. 1991, doi: 10.1029/91JC00302.

[3] F. C. Jackson, "An Analysis of short pulse and dual frequency radar techniques for measuring ocean wave spectra from satellites," *Radio Sci.*, vol. 16, no. 6, pp. 1385–1400, Nov. 1981, doi: 10.1029/RS016i006p01385.

[4] D. Hauser *et al.*, "New Observations from the SWIM Radar On-Board CFOSAT: Instrument Validation and Ocean Wave Measurement Assessment," *IEEE Trans. Geosci. Remote Sens.*, vol. 59, no. 1, pp. 5–26, 2021, doi: 10.1109/TGRS.2020.2994372.

[5] E. Le Merle *et al.*, "Directional and Frequency Spread of Surface Ocean Waves From SWIM Measurements," *J. Geophys. Res. Ocean.*, vol. 126, no. 7, 2021, doi: 10.1029/2021JC017220.

[6] G. Liang, J. Yang, and J. Wang, "Accuracy Evaluation of CFOSAT SWIM L2 Products Based on NDBC Buoy and Jason-3 Altimeter Data," *Remote Sens.*, vol. 13, no. 5, p. 887, Feb. 2021, doi: 10.3390/rs13050887.

[7] H. Jiang, A. Mironov, L. Ren, A. V. Babanin, J. Wang, and L. Mu, "Validation of Wave Spectral Partitions From SWIM Instrument On-Board CFOSAT Against In Situ Data," *IEEE Trans. Geosci. Remote Sens.*, vol. 60, pp. 1–13, 2022, doi: 10.1109/TGRS.2021.3110952.

[8] B. Li *et al.*, "Calibration Experiments of CFOSAT Wavelength in the Southern South China Sea by Artificial Neural Networks," *Remote Sens.*, vol. 14, no. 3, pp. 1–23, 2022, doi: 10.3390/rs14030773.

[9] C. Tourain and D. Hauser, "SWIM PRODUCTS USERS GUIDE Product," 2018

[10] NDBC Web Data Guide, "NDBC Web Data Guide," *Stennis Space Center*, 2015.

[11] A. Lygre and H. E. Krogstad, "Maximum entropy estimation of the directional distribution in ocean wave spectra," *Deep Sea Res. Part B. Oceanogr. Lit. Rev.*, vol. 34, no. 9, p. 736, Jan. 1986, doi: 10.1016/0198-0254(87)90046-X.

[12] G. Huffman, D. Bolvin, D. Braithwaite, K. Hsu, and R. Joyce, "NASA Global Precipitation Measurement (GPM) Integrated Multi-satellitE Retrievals for GPM (IMERG)," *Nasa*, no. December, p. 29, 2019, [Online]. Available: https://pmm.nasa.gov/sites/default/files/document_files/IMERG_ATBD_V06.pdf

[13] D. Hauser, C. Tison, T. Amiot, L. Delaye, N. Corcoral, and P. Castillan, "SWIM: The First Spaceborne Wave Scatterometer," *IEEE Trans. Geosci. Remote Sens.*, vol. 55, no. 5, pp. 3000–3014, 2017, doi: 10.1109/TGRS.2017.2658672.

[14] C. Tourain *et al.*, "Benefits of the Adaptive Algorithm for Retracking Altimeter Nadir Echoes: Results From Simulations and CFOSAT/SWIM Observations," *IEEE Trans. Geosci. Remote Sens.*, vol. 59, no. 12, pp. 9927–9940, Dec. 2021, doi: 10.1109/TGRS.2021.3064236.

[15] F. Ardhuin *et al.*, "Semiempirical dissipation source functions for ocean waves. Part I: Definition, calibration, and validation," *J. Phys. Oceanogr.*, vol. 40, no. 9, pp. 1917–1941, 2010.

[16] P. A. Hwang, "Comment on 'A study of the slope probability density function of the ocean waves from radar observations' by D. Hauser et al.," *J. Geophys. Res.*, vol. 114, no. C2, p. C02008, Feb. 2009, doi: 10.1029/2008JC005005.

[17] D. Hauser, G. Caudal, S. Guimbard, and A. Mouche, "Reply to comment by Paul A. Hwang on 'A study of the slope probability density function of the ocean waves from radar observations' by D. Hauser et al.," *J. Geophys. Res.*, vol. 114, no. C2, p. C02009, Feb. 2009, doi: 10.1029/2008JC005117.

[18] H. Mitsuyasu *et al.*, "Observations of the Directional Spectrum of Ocean WavesUsing a Cloverleaf Buoy," *J. Phys. Oceanogr.*, vol. 5, no. 4, pp. 750–760, Oct. 1975, doi: 10.1175/1520-0485(1975)005<0750:OOTDSO>2.0.CO;2.

[19] G. Z. Forristall and K. C. Ewans, "Worldwide Measurements of Directional Wave Spreading," *J. Atmos. Ocean. Technol.*, vol. 15, no. 2, pp. 440–469, Apr. 1998, doi: 10.1175/1520-0426(1998)015<0440:WMODWS>2.0.CO;2.

[20] M. Donelan, A. Babanin, E. Sanina, and D. Chalikov, "A comparison of methods for estimating directional spectra of surface waves," *J. Geophys. Res. Ocean.*, vol. 120, no. 7, pp. 5040–5053, Jul. 2015, doi: 10.1002/2015JC010808.

> <

[21] M. Benoit, P. Frigaard, and H. A. Schaffer, “Analyzing multidirectional wave spectra,” in *Iahr Congress*, 1997, no. January 1997, pp. 131–158.

[22] D. E. Hasselmann, M. Dunckel, and J. A. Ewing, “Directional Wave Spectra Observed during JONSWAP 1973,” *J. Phys. Oceanogr.*, vol. 10, no. 8, pp. 1264–1280, Aug. 1980, doi: 10.1175/1520-0485(1980)010<1264:DWSODJ>2.0.CO;2.

[23] E. Peral, E. Rodríguez, and D. Esteban-Fernández, “Impact of surface waves on SWOT’s projected ocean accuracy,” *Remote Sens.*, vol. 7, no. 11, pp. 14509–14529, 2015, doi: 10.3390/rs71114509.

[24] W. C. O’Reilly, T. H. C. Herbers, R. J. Seymour, and R. T. Guza, “A Comparison of Directional Buoy and Fixed Platform Measurements Of Pacific Swell,” J. Atmos. Ocean. Technol., vol. 13, no. 1, pp. 231–238, Feb. 1996, doi: 10.1175/1520-0426(1996)013<0231:ACODBA>2.0.CO;2.

[25] N. D. Longuet-Higgins, M. S. and Cartwright, D. E. and Smith, Observations of the directional spectrum of sea waves using the motions of a floating buoy. 1963.

[26] E. Le Merle, D. Hauser, and C. Tison, “Directional wave spectra at the regional scale with the KuROS airborne radar: comparisons with models,” Ocean Dyn., vol. 69, no. 6, pp. 679–699, 2019, doi: 10.1007/s10236-019-01271-5.